
University of Oldenburg

Neurocognitive Psychology (M. Sc.)

Master's Thesis

Title:

***Parkinson's Disease and Olfaction: A Resting State fMRI and Brain Morphometry Investigation***

Presented by: Kathryn Ann Beard

First Examiner: Dr. Peter Sörös

Second Examiner: Prof. Dr. Jochem Rieger

Oldenburg, 11.09.2019

# Abstract

**Introduction:** Parkinson's disease (PD) is a debilitating and prevalent neurodegenerative disease affecting around 1% of the population over the age of 60. The exact cause in most cases is unknown. One common non-motoric symptom of PD is hyposmia; a dysfunction of olfaction. This symptom precedes most motor symptoms and is highly correlated with cognitive decline. The present study aims to determine if alterations in resting-state networks (RSN) and brain structure correlate with hyposmia and/or PD. It is predicted that PD patients with severe hyposmia will display changes in brain connectivity within and between RSNs compared to the control group.

**Methods:** 45 cognitively normal volunteers underwent an fMRI scan at rest. 15 participants were healthy controls, 15 were PD patients with severe hyposmia, and 15 were PD patients with no/mild hyposmia. Hyposmia was assessed based on scores from a smell recognition test (OSIT-J). The data was measured and publicized by Yoneyama et al. (2018). An ICA-based analysis method with a low dimensionality specification, in combination with dual-regression was utilized to identify interpretable RSNs and compare them between participants with additional regressors. Freesurfer software was selected to produce both cortical thickness and subcortical volume median values for each participant's structural brain image.

**Results:** The results of these analyses support the null hypothesis. There were no significant differences in any independent components reflective of canonical RSNs between groups, or within the entire group related to smelling scores or cognition. The median volumes for several subcortical regions and median thickness values of cortical regions were statistically independent from the clinical effects of PD and hyposmia in this study ($p > 0.05$).

**Discussion:** The results of the ICA combined with dual-regression analysis reject the hypothesis that there would be significant changes in RSNs as a consequence PD pathology and hyposmia, and there were also no reportable differences in brain morphometry. This suggests that PD patients on medication maintain strikingly intact RSNs and brain structure. This result could alternatively be attributed to a number of methodological study limitations. The same dataset in the Yoneyama et al. (2018) study yielded several significant results between group RSNs and cortical thickness values. Thus, the results presented here highlight a reoccurring issue: MRI replication studies applying alternative methodological choices to the same data can produce rather varied results. The neuroimaging of potential changes related to PD, dopamine regulatory medications, and hyposmia, requires further attention.

# Contents

# Abbreviations List

| | |
|---|---|
| ACE-R | Addenbrooke's Cognitive Examination- revised |
| AD | Alzheimer's Disease |
| ADHD | Attention deficit hyperactivity disorder |
| ANCOVA | Analysis of covariance |
| ANOVA | Analysis of variance |
| ANTs | Advanced Normalization Tools software |
| AON | Anterior olfactory nucleus |
| BET | Brain extraction tool |
| BOLD | Blood-oxygen-level dependent |
| CSF | Cerebrospinal fluid |
| CNS | Central nervous system |
| DA | Dopamine |
| DAN | Dorsal attentional network |
| DMN | Default mode network |
| FC | Functional connectivity |
| fMRI | Functional magnetic resonance imaging |
| FOV | Field of view |
| GICA-DR | Group independent component analysis- dual regression |
| GLM | General linear model |
| HC | Healthy control |
| ICA | Independent component analysis |
| IC | Independent component |
| L-Dopa | Levodopa |
| LEDD | Levodopa equivalent daily dose |
| MDS | Movement Disorder Society |
| MDSUPDRS | Movement Disorder Society-Sponsored Revision of the Unified Parkinson's Disease Rating Scale |
| MMSE | Mini Mental State Exam |
| MNI | Montreal Neurological Institute |
| MRI | Magnetic resonance imaging |
| MS | Multiple Sclerosis |
| OASIS | Open access series of imaging studies |
| OSIT-J | Odor stick identification test for the Japanese |
| PD | Parkinson's Disease |
| PD/MH | Parkinson's Disease with mild or no hyposmia |
| PD/SH | Parkinson's Disease with severe hyposmia |
| PET | Positron-emission tomography |
| rsfMRI | Resting-state functional magnetic resonance imaging |
| RSN | Resting-state network |
| SCA | Seed-based correlation analysis |
| SD | Standard deviation |
| SPM | Statistical parametric mapping |
| TDI | Odor threshold, discrimination, and identification |
| TE | Echo time |
| TR | Repetition time |
| UPSIT | University of Pennsylvania smelling identification test |

# 1 Introduction

## 1.1 Parkinson's Disease

James Parkinson is the man regarded for coherently categorizing and describing the deadly and prevalent disease that is now his namesake. It is quite remarkable that even in 1817 Parkinson felt the unyielding need to differentiate between certain types of tremor. In doing so, he discovered a vigorous method for discriminating between his illness of interest, the "Shaking Palsy", and other ailments that can cause trembling. His writings elaborately describe symptoms and other observations relative to the pathognomy; additionally, Parkinson even makes a prediction that the disease is a dysfunction of the CNS rather than the PNS. His suggestion about the specific anatomical regions underling the disease pathology is now understood to be false, however, with regard to the time period and lack of noninvasive imaging technology his prediction is still highly respected. His groundbreaking essay on the shaking palsy paved the way for over 200 years' worth of research on this debilitating malady. It was James Parkinson's demand that the disease's "real nature may be ascertained, appropriate modes of relief, or even a cure, pointed out." (Parkinson, 1817/2002, pp. 236).

These many years of follow up research have only partially satisfied the ambitions of James Parkinson. To date, Parkinson's Disease (PD) is categorized as a chronic, progressive, adult-onset neurodegenerative disease that has no cure. The cause of the disease is also unknown in most cases. There have been several reported genetic and environmental risk factors; nonetheless the disease still remains overwhelmingly idiopathic. PD affects around 1% of the population over 60-years-old and roughly 4% of those over the age of 80. The duration of the disease can last between 7-14 years on average; symptoms increasing in severity lead to death indirectly (Sveinbjornsdottir, 2016). Fortunately, dedicated researchers have been able to shed light on the specifics of the disease's pathology, motor and non-motor symptoms, as well as possible treatment methods.

The symptoms of PD are divided into two main categories: motor and non-motor. The motor symptoms are generally the hallmark indications of the

disease. The Movement Disorder Society (MDS) provides specific diagnostic guidelines for identification of these motor symptoms that are described as: Bradykinesia in combination with rigidity, resting tremor, or both. Bradykinesia is defined specifically as slowness in initiating movement accompanied by progressively diminished speed/amplitude with each motor repetition (Postuma et al., 2015). These motor symptoms also progressively become worse but can be treated. Most commonly, motor symptoms are treated with L-Dopa, which is a precursor to the neurotransmitter dopamine (Emamzadeh & Surguchov, 2018)

The etiology of these motor symptoms related to PD can be thoroughly explained as the direct result of dopaminergic neuron death within the substantia nigra. The substantia nigra is a collection of subcortical nuclei, part of the basal ganglia, located in the midbrain. It contains two parts, the pars reticulata and the pars compacta, each with different functions and connections. The pars reticulata receives projections from the striatum and sends inhibitory signals to the thalamus via GABAergic neurons. The pars compacta, the region affected most in PD, contains mostly dopaminergic neurons that project excitatory signals onto the striatum. When PD related cell death occurs in this region, it disrupts the nigrostriatal pathway which is responsible for initiating and calibrating movements. This disruption of a major motor pathway directly explains why the motor dysfunctions occur. However, the cause underlying the substantial death of these DA neurons is not directly known (Schapira, 2006). Histopathologists have consistently observed infestations of Lewy bodies within the substantia nigra and other brain regions of PD patients. The role of these Lewy bodies, which are tangles made up of mainly alpha-synuclein proteins, are still very much unclear (Gibb et al., 1988; Schapira, 2006; Doty, 2012).

The non-motor symptoms of PD tend to be somewhat overshadowed by the more obvious motor symptoms, although by some they are considered to be equally as debilitating. These non-motor manifestations are numerous, and broadly categorized as: sleep dysfunction, autonomic dysfunction, psychiatric dysfunction, and hyposmia. Autonomic problems tend to be mainly gastrointestinal, however drops in blood pressure, sexual dysfunction, excessive sweating, and other symptoms are also reported. Sleep cycle abnormalities are

also observed in two thirds of PD patients, along with chronic daytime sleepiness. The psychiatric problems that arise as a result of PD, independent of the medication induced side effects are: visual hallucinations, depression, anxiety, and dementia. Some of these non-motor symptoms make an appearance long before the first noticeable tremors reveal themselves (Sveinbjornsdottir, 2016). This means that understanding that the pathological changes pertaining to these non-motor occurrences, is of clinical importance. Diagnostic procedures rely on such research. The last category of non-motor symptoms that can present up to 10 years before motor symptoms is hyposmia (Baba et al. 2011).

## 1.2 Hyposmia and Smell Tests

The partial to complete loss of smelling capabilities, hyposmia, is a relatively common sensory disorder that tends to worsen with age (Murphy et al., 2002). Hyposmia also decreases taste perception, can be an issue of safety, and can be brief or permanent depending on the specific cause. The causes of hyposmia are most commonly a result of direct problems with the nose or sinuses, such as severe allergies, influenza, nasal polyps, exposure to chemicals, or injury to the head/nose. Medications can sometimes also cause a loss of smell. These factors are usually responsible for a brief loss of smell that eventually returns to normal. There are some cases though, where hyposmia occurs in combination with more serious, long-term conditions. Several studies have shown a relationship between hyposmia and dementia, frontotemporal dementia, Alzheimer's disease (Franks et al., 2015), PD (Yoneyama et al., 2018; Baba et al., 2011; Bohnen et al., 2008; Doty, 2012), multiple sclerosis, type 1 diabetes, and Lewy Body disease. When hyposmia occurs suddenly and without an obvious cause, it could very well be an ominous sign of neurological malfunction (Goncalves & Goldstein, 2016). Hyposmia is diagnosed first by a physician's physical examination in combination with medical history, and if no obvious source can be established, a diagnosis can be made using MRI (Yousem et al., 1996), a smell stick test (Kobal et al. 1996; Hummel et al., 1997/2007), or a scratch and smell test (Doty et al., 1984).

A smell stick test is conducted with a pen-like device that can release a certain smell at varied amounts. A scratch and smell test on the other hand, is a paper test where odors are exposed after scratching off a microencapsulated seal. These types of tests are also efficacious for collecting a smelling score in experimental settings, including the study that provided their data for the present investigation. These nasal chemosensory odor identification batteries, which have additionally been developed for different countries with different familiar odors, can reliably provide an overview of an individual's ability to identify familiar smells, ability to discriminate between different smells, and at which threshold odors are first perceived. The smell stick measures compile to provide a TDI score. The modern "Sniffin' Sticks" test battery developed by Kobal, Hummel, and colleagues in 1996 is commonly used to diagnose hyposmia, anosmia, or normosmia based on a collection of normative data from well over 3000 participants (Kobal et al., 1996). The UPSIT, or the University of Pennsylvania Smell Identification Test, was developed in 1984 by Doty and colleagues and is currently the most widely used tool for olfaction sensory measurements in the world. It is available in 28 languages with several international variations and can be self-administered. This test is also considered to be very valid with test-retest reliability of 0.94 (Doty, 2012).

These smell tests are considered quite reliable in the diagnosis of hyposmia and other dysfunctions of smelling within healthy populations. However, in recent years there has also been some criticism over whether or not the tests accurately measure odor sensation and perception as well as previously reported in clinical populations. In recent publications, the sensitivity and specificity measures regarding the UPSIT and similar brief international tests' abilities to diagnose PD have been lower than expected. Rodriguez-Violante et al. (2014) reported the UPSIT sensitivity to be 79.7% and sensitivity to be 68.5% using a cut off score of >=25 for Mexican participants. The ability for the test to diagnose PD patients was calculated to be with 75.3%. These lower than expected findings may be due either to cultural limitations, or something physiological (Rodriguez-Violante et al., 2014).

Another method being used to potentially identify the presence of hyposmia or smell dysfunction is MRI analysis, in both task and resting

conditions. Yousem et al. (1996) found that those with hyposmia or anosmia from birth, 68-84% showed a nearly compete loss of the olfactory bulb and tract. In addition to some observable subcortical biomarkers, in 2010 Bitter and colleagues used neuroimaging to observe gray matter and white matter morphometric differences. Astoundingly they report significant loss of both gray and white matter volume in the brains of hyposmic/anosmic patients as compared to age-matched controls; the following regions with significant gray matter differences were: insular cortex, anterior cingulate cortex, orbitofrontal cortex, cerebellum, fusiform gyrus, precuneus, middle temporal gyrus and piriform cortex. The regions of the brain that displayed white matter volume loss were under the insular cortex and middle frontal gyrus, as well as in the cerebellum (Bitter et al., 2010). To better understand these changes, a brief background on olfactory cortical and subcortical neuroanatomy and pathways is provided in the following section.

### 1.3 Olfaction Basics

The human chemosensory sense of smell is astonishing to say the very least, for our smelling capabilities possess the potential to discriminate between trillions of tiny molecular combinations. A review article written by biologist Stuart Firestein (2001) outlines the basics of the olfactory system in humans and similar mammals. Firestein states firstly that there are two different olfactory systems at play in most animals: the first primary system is mostly conscious and consists of detecting food smells, rot, danger, and other scents necessary to stay alive; the other secondary system that is less conscious in humans is for smelling out a potential receptive mate. In relevant reference to the present study, the overview of the anatomical organization of the olfactory system will be strictly limited to the primary sense of smell within humans.

The first noteworthy peripheral structure is the olfactory neuroepithelium, which is a patch of mucus covered skin about $10cm^2$ located at the uppermost part of the nasal cavity. This epithelium is covered with 10 to 20 million olfactory sensory cells that come in an estimated six different types. These bipolar neurons detect and respond to molecular combinations present in odor molecules, with the purpose of sending along these unique molecular

codes through a thin part of the skull (cribriform plate) to the outer layer of the olfactory bulb. This olfactory bulb and its tract are some of the most anatomically recognizable structures located bilaterally on the inferior forebrain. The olfactory bulb is the transduction hub, where olfactory sensory cells send their complex chemical codes of detected molecules to converge, firstly, on round glomeruli cells. These cells are spatially organized to integrate and simplify the sensory input, that is then passed on through a layer of mostly interneuron, to mitral cells, and then to the olfactory tract. These mitral cells are few, but their function within the olfactory bulb and tract are highly complex and essentially, they integrate the odor sensations in order to transport them for quick perception (Blumenfeld, 2010; Firestein, 2001).

The olfactory tract transports signals to a number of other cortical and subcortical regions. The five main ones being: the anterior olfactory nucleus (AON), olfactory tubercle, amygdala, piriform cortex, and entorhinal cortex. The AON projects inhibitory signals back onto the olfactory bulb, while the piriform cortex is responsible for identifying characteristics of the odor in terms of both its chemical structure and similar categorical properties. The piriform cortex sends projections to a number of different regions, including: thalamus, hypothalamus, amygdala, hippocampus, and orbitofrontal cortex. One particular pathway sends signals from the piriform cortex to the mediodorsal nucleus of the thalamus, and then to the orbitofrontal cortex for conscious processing. The entorhinal cortex's projections of odor signals on the amygdala and hippocampus are well-known for providing us with emotional, memory, and autonomic responses to smells. The olfactory system is anatomically close to to the limbic system, which could explain why smells can sometimes evoke strong emotional memories (Blumenfeld, 2010).

These complex inner workings of olfaction make it sometimes difficult to understand the root and pathology of olfactory dysfunctions. With the puzzling connection between smell dysfunction and neurodegenerative disease, it is of great importance to understand the olfactory system's healthy characteristics and functions. Then we may better be equipped to find neurophysiological warning signs in the future. One hope that researchers have is the availability

and growing popularity of clinical MRI research, such as resting state and brain morphometry.

## 1.4 Resting-State fMRI

Functional magnetic resonance imaging of the brain has completely revolutionized the way medical professionals and researchers understand both the normal and abnormal structure and functioning of the human brain. Since the beginning of the 1990's, the use of fMRI in experiments has exploded and today there are now well over 5,000 studies published mentioning fMRI in the title. This popularity is due to its non-invasive and relatively quick data acquisition which produces results of excellent spatial resolution. The temporal (time) resolution is also not awful, and data analysis can also be completed rather effortlessly with the current array of available fMRI analysis software packages (Poldrack et al., 2009). These software packages, such as FSL (FMRIB's Software Library) and SPM (Statistical Parametric Mapping), allow raw fMRI data to be preprocessed and statistically analyzed, so that the changes in the brain's blood oxygenation levels may be visualized and statistically interpreted as changes in localized brain activation.

The result of fMRI studies is either a spatial map statistically representing localization of brain function in response to stimuli or a spatial map of intrinsic connectivity. Resting-state fMRI (rsfMRI) is a subfield of fMRI analysis that focuses exclusively on what happens in the brain independent of performing tasks, during "rest". Therefore, rsfMRI can provide images reflective of brain connectivity, which can be measured with the assumption that: brain regions that spontaneously activate with similar signals at different spatial locations at around the same time are functionally connected. At times interpretation may be difficult because connected brain regions may not always influence each other directly, but rather indirectly, or there may be another brain region that has an unnoticed influence. Nonetheless, fMRI analysis of human participants and patients at rest is very important for establishing a baseline of brain functioning.

The past years of rsfMRI have provided a more comprehensive list of different brain connectivity networks, called resting state networks (RSN),

which are observably active during rest and lessen in activation during task performance. The most notable RSN in terms of its consistent reproducibility is the default mode network (DMN) which includes the connected brain areas: posterior cingulate cortex, precuneus, medial prefrontal cortex, inferior parietal lobule, and lateral temporal cortex. In contrast, a task related network called the dorsal attention network (DAN), correlates negatively with the DMN and it contains regions associated with goal-oriented behavior. Utilizing rsfMRI as a tool to observe reproducible maps of activation has several potential clinical implications as well, because changes in these "baseline" networks could signal a potential neurological and/or psychological dysfunction (Bijsterbosch et at., 2017; Yeo et al., 2011).

The usage of rsfMRI in clinical practice has the promising potential to provide biomarkers for certain neuropsychological diseases and disorders. Biomarkers are consistent observable measures of a normal medical state, and with these it is possible to compare and categorize different states as pathological. In the realm of neuropsychology, comparing normal RSNs to seemingly abnormal RSNs could help medical professionals to accurately and swiftly identify indications of diseases and disorders such as: Alzheimer's disease (AD), PD, dementia, schizophrenia, anxiety, post-traumatic stress, ADHD, autism, and many more. A prime example of this was found by researcher Koch and colleagues (2010), in a study they conducted attempting to find a good analysis method for accurately diagnosing AD using resting state fMRI data. The researchers found that using a combination of Independent Component Analysis (ICA) -based techniques with time course correlation analyses enabled the categorical separation of healthy controls from AD patients; the reported accuracy was 97.2%, with sensitivity 100% and specificity 95.2% (Koch et al. 2010).

When rsfMRI is utilized to examine the brains of PD patients, interesting findings have been reported. Ghahremani et al. published research in 2018 reporting differences in connectivity outside of the motor networks. Motor network alterations in PD patients compared to controls are commonly observed and also unsurprising (Wu et al., 2009), however changes in the DMN, for example, are very intriguing to find. Ghahremani and colleagues

used a seed-based correlation analysis as well as a novel persistent homology method to observe decreased global connectivity in PD patients off medication compared to controls both within and outside of the DMN. They also reported an increase in local brain connectivity in PD patients, and they concluded that these widespread connectivity differences are an indication that PD impacts the functioning and connectivity of the entire brain (Ghahremani et al., 2018). The following section overviews another method of MRI analysis used in the present study, brain matter morphometry.

## 1.5 Brain Morphometry

The human brain is nearly as individual to every person as their own finger print, with varying sulci, gyri, and subcortical structures. Today is it actually relatively easy to observe every different brain's architecture with sharp detail. MRI machines of 3-Tesla and higher provide detailed anatomical brain images, which in turn makes it possible for researchers to study the size and shape of the brain as a whole or in segregated parts. This computational method of measuring brain tissue is called brain morphometry, and today it is widely used as a tool for finding abnormal anatomical differences that consistently reflect the effects of aging, gender, the environment, disease, disorder, genetics, and more. MRI brain tissue measurements can be produced for both cortical and subcortical regions by utilizing one of two major modern methods: voxel-based or surface-based morphometry (Clarkson et al., 2011). There are other methods such as deformation and tensor-based morphometry, however they will not be further mentioned in this paper.

### 1.5.1 Cortical Measures

Voxel-based morphometry is the slightly older method of the two, first mentioned in 1995 (Wright et al.) and then the methods were updated and coherently standardized in 2000 (Ashburner & Friston). Surface-based morphometry is a more complex computational method that arose to combat some limitations of the voxel-based methods. Both measurement strategies involve a segmentation algorithm that separates the white matter, gray matter, and cerebrospinal fluid (CBF) using brightness/intensity values, as well as some form of image registration/normalization. Voxel-based methods use

preprocessed anatomical images and each individual voxel within a subject's brain, to allow a statistical comparison of cortical size, thickness, volume, density etc. Voxel-based morphometry is straightforward and simple; however, voxels are geometric cubes with rather indirect biological interpretability, thus the method can be vulnerable to inaccuracies in terms of localization (Clarkson et al., 2011; Tucholka et al., 2012). Surface-based morphology on the other hand is more complex computationally. Essentially the method and algorithms produce cortical volume, thickness, and surface area measures by applying a triangular mesh surface model to both the pial and white matter cortical boundaries based on within-subject co-registration of common cortical folding patterns (Fischl, 2012; Tucholka et al. 2012).

Full, coherent comparisons and explanations of voxel/surface-based cortical morphometry methods are rather lengthy, but the main concept is that surface-based methods are more complex and have been consistently reported to be more sensitive and reliable than voxel-based methods (Clarkson et al., 2011; Greve, 2011; Fischl, 2012; Tucholka et al. 2012). Surface-based methods are used in the present investigation to produce cortical thickness values and will therefore be further explained. The most popular software for completing surface-based cortical morphometry is Freesurfer (Fischl, 2012), which was developed in order to easily apply necessary algorisms and deformations to several input T1-weighted anitomical images. Freesurfer has been used to observe morphometrical differences between subjects and groups for the last decade with high reliability and spatial accuracy. Diseases and ageing are generally responsible for most of the noticeable cortical thickness changes in humans, and Freesurfer cortical analysis has been reported to be very useful in detecting such changes (Fischl, 2012; Fjell et al., 2006; Righart et al., 2017). A recent 2018 study by Radziunas and colleagues used the software to find significant cortical thickness differences in PD patients relative to their specific manifestations of sleep disturbances. A study in 2016 by Geritts and researches reported cortical thickness and surface area changes in PD patients compared to controls both in general and in relation to cognition. These are just two examples, but the point remains that Freesurfer is a widely used cortical and

valid measurement tool with several clinical applications (Geritts et al., 2016; Radziunas et al., 2018).

### 1.5.2 Subcortical Measurements

The process of quantifying the brain in terms of volume becomes more complicated below the cortex. Subcortical brain regions such as parts of the basal ganglia, the amygdala, thalamus, hippocampus, etc. can be varying in density with tissue borders seeming rather arbitrary. Segmentation and categorization of subcortical structures may be done manually or automatically. Scan-rescan reliability measures based on automatic segmentation tend to be much lower for subcortical structures, but manual segmentation is unfortunately very time consuming and impractical (Morey et al., 2010). Freesurfer developers decided to program the segregation of the subcortical brain into 40 interpretable structures by designing an automatic process in which every single voxel in the individual's normalized brain is categorized based on a probability atlas they constructed. This voxel-based method is very pragmatic and interpretable, and like cortical methods, has several clinical and applied benefits (Fischl, 2012).

Changes in subcortical volumes have been reported in several clinical populations such as AD patients, schizophrenic patients, severely depressed individuals, and many additional groups. A 2015 article published in *Nature: Molecular Psychiatry* reported findings by van Erp et al., which were a comprehensive list of subcortical regions affected by schizophrenia, based on a sample size of over 2,028 patients and 2,540 healthy controls. This study used Freesurfer's automatic segmentation to find that schizophrenic patients display decreased volume in the amygdala, hippocampus, thalamus, and accumbens as well as increased volumes in the ventricles and pallidum (van Erp et al., 2015). Subcortical changes in PD, however, are less prominent with some studies reporting no significant findings. Messina and colleagues (2011) used Freesurfer's segmentation to search for subcortical differences between PD patients, multiple system atrophy patients, progressive supranuclear palsy patients, and healthy controls. The researchers found several subcortical

atrophies in all clinical groups except for the PD group, which produced no significant differences at all (Messina et al., 2011).

## 1.6 Parkinson's Disease and Olfaction

The puzzling connection between PD and its common and early-onset olfactory symptom is one that should be investigated thoroughly. However, brain activity and structural changes due to the non-motor symptoms of PD, specifically hyposmia, can be rather complicated to observe with MRI. Very few studies have attempted to find an observable relationship between the hyposmia and PD, regardless of the potential clinical benefits, because imaging studies already have been reporting inconsistent results when imaging PD pathology alone. A meta-analysis published in 2017 assembled brain imaging attempts to find PD biomarkers, and the results were quite direct: rsMRI/structural MRI studies aiming to successfully distinguish PD patients from healthy controls, rarely produce significant findings unless the PD patients are already further along in disease progression and/or off medication at the time of scanning. Unfortunately, if PD cannot be consistently imaged and identified in the early pre-motor stages, the opportunity to utilize rsMRI or brain morphometry as a diagnostic tool diminishes (Tuite, 2017). By all means, there are a few task-based fMRI and PET studies reporting significant findings related to olfaction and PD, but they are few indeed (Hummel et al., 2010; Su et al., 2015; & Westermann et al., 2008). Hummel et al. (2010) for example, found significant activity decreases in the amygdala, hippocampus, and ventral striatum in PD patients compared to controls when introduced to odors in the scanner. Even though there are limited publications exhibiting notable brain changes in PD patients with hyposmia, there is still optimism for future findings as MRI technology and analysis methods consistently evolve.

Some structural and functional MRI research in recent years has been able to display some results identifying brain changes related to cognitive decline in PD patients (Doty, 2012). Other studies have also reliably reported that severely hyposmic PD patients have a much greater chance to also develop or possess cognitive and psychotic symptoms. Morley et al. in 2011, found a strong correlation between PD patients with hyposmia and executive

functioning deficits, memory deficits, and psychostic symptoms. They then concluded that hyposmia is pathognomonic of other nonmotor symptoms, and it may not only serve as a pre-diagnostic biomarker for PD, but also as an indication for disease progression and development of more debilitating nonmotor symptoms. (Morley et al., 2011). Since the nature of olfactory dysfunction is both a failure of sensory and cognitive systems, with very strong correlations to other aspects of cognition, imaging hyposmia in PD patients could yield groundbreaking clinical interpretations. For example, MRI as a tool to calculate the potential risk of PD patients developing mild cognitive impairments or even dementia (Baba et al., 2012; Fullard et al., 2016; Morley et al., 2011).

### 1.6.1 Yoneyama et al. 2018 study

The rapidly growing clinical attention to resting state fMRI and structural brain morphometry sparks hope to an approaching revelation of clear understanding about the manifestation of neurological and psychological disease in greater detail. To date, the olfactory functioning in PD patients has rarely demonstrated observable significant alterations in brain connectivity or tissue atrophy. One exception is the paper that provided the data for the present study. Yoneyama and colleagues performed three types of analyses on the brain scans of 45 cognitively normal participants, a third of which were healthy age-matched controls, a third were PD patients with mild or no hyposmia, and finally a third of the group were PD patients with severe hyposmia. More information on the patient demographics and categorization methods can be found in the methods section 2.1. The analysis methods selected by Yoneyama et al. were a cortical grey matter volume analysis and both a seed-based correlation connectivity analysis as well as a whole brain canonical resting state fMRI connectivity analysis (Yoneyama et al., 2018).

The results of the voxel-based grey matter volume comparison displayed significant increases and decreases in grey matter between controls and the PD group with severe hyposmia. The decreases were observed in the PD hyposmia group in the following regions: “the bilateral cuneus, right associative visual area, precuneus, middle temporal gyrus, superior frontal

gyrus, middle frontal gyrus, inferior frontal gyrus corresponding to the operculum, superior temporal gyrus, precentral gyrus, and middle temporal gyrus" (Yoneyama et al. 2018, pp. 6). The grey matter volume increases were reported in the posterior insula and surrounding regions in the brains of the PD severe hyposmia patients, and the changes were also significantly correlated to their smelling scores. These increase volume findings were also significant when compared to the PD group with hyposmia. *Figure 1* is a visual representation of the significantly different clusters. The interpretation provided by Yoneyama and colleagues for these decreases were that these affected brain regions correlate to higher level olfactory functioning in terms of odor intensity and quality discrimination, odor recognition, and passive smelling. The reported increase in grey matter, however, is a bit more abstract and difficult to explain (Yoneyama et al., 2018).

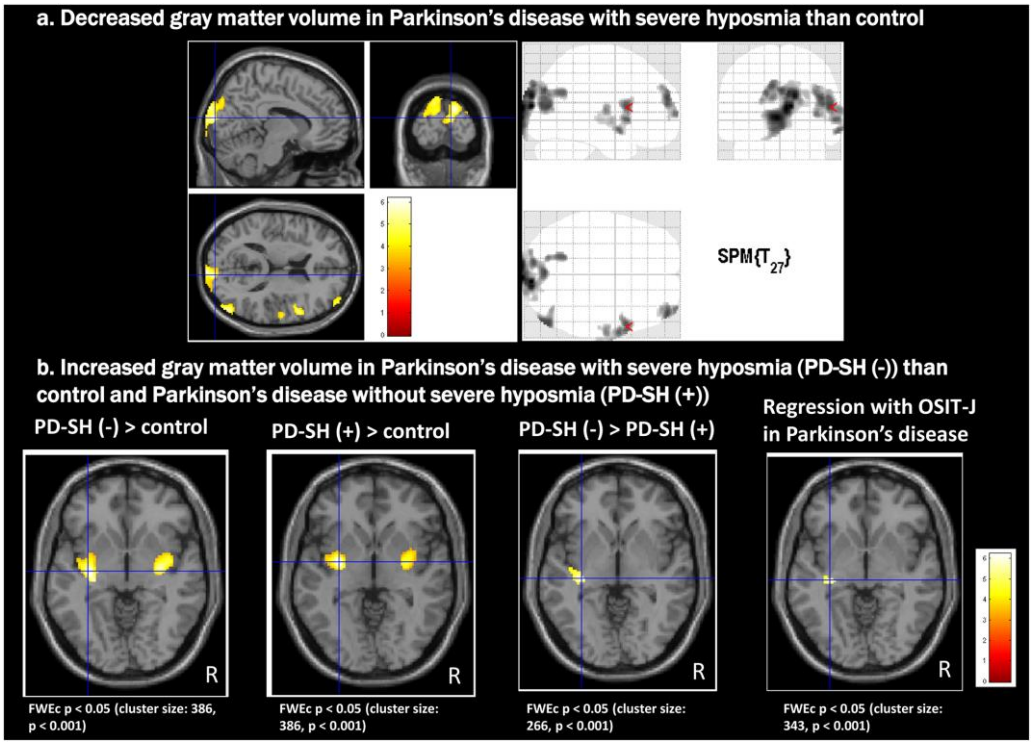


*Figure 1*: the grey matter volume decreases and increases reported by Yoneyama et al. (2018) can be observed above. The yellow clusters are significantly different in size between groups ($p < 0.05$) after the family-wise-error correction for multiple comparisons, and the cluster significance threshold is set to $p < 0.001$. (Yoneyama et al. 2018, pp. 7; Fig 1)

The results of Yoneyama's seed-based correlation analysis (SCA) were quite notable, with significant and widespread changes in connectivity between the

three nuclei of the amygdala "seeds" and several other brain regions. These differences of decreases and increased functional connectivity were observed between the PD patients with severe hyposmia and the healthy control group. There were also mild significant connectivity decreases between the PD group with severe hyposmia and the PD group without. These findings were also examined with dual-regression and were significantly correlated with individual smelling and cognitive performance scores (Yoneyama et al., 2018).

Finally, Yoneyama et al. applied a data-driven ICA analysis paired with dual-regression to search for and discover changes in canonical resting state brain network connectivity. They uncovered a decrease in connectivity between controls and PD Patients with severe hyposmia within the precuneus network, as well as an increase in connectivity within the high and primary visual networks. Both of these findings were significant ($p < 0.05$). Significant changes between controls and PD hyposmic patients were also reported between several canonical networks and brain regions outside of these networks (Yoneyama et al., 2018). These significant results will be presented in *Figure 2*.

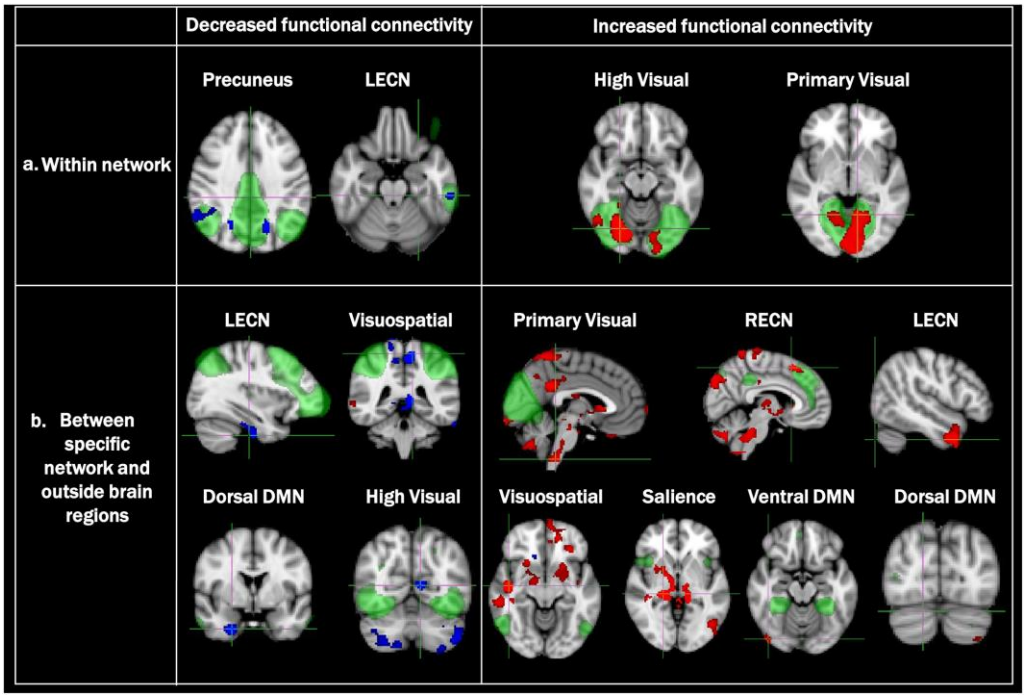


*Figure 2*: These are the GICA-DR rs-fMRI results reported from the Yoneyama et al. 2018 paper. In section *a*, above, the within network functional connectivity changes can be observed, both increases and decreases. In section *b* the between network connectivity alterations are also presented. The significant between group differences ($p < 0.05$) are only between the HC and PD/SH, and are corrected for multiple comparisons (Yoneyama et al., 2018, pp. 10).

### 1.6.2 Hypotheses

The study by Yoneyama et al. (2018) published novel and astonishing significant differences between control participants, and cognitively normal PD patients with and without severe olfactory deficits. The authors were helpful in providing public access to their study data that is analyzed in the present study. Lack of prior, consistent results in the search for seemingly elusive statistical differences in brain structure and connectivity in PD patients with and without olfactory deficits, make the task of choosing analysis methods and forming hypotheses rather daunting. It must first be noted, that the present study is by no means an exact/direct replication study, conversely it is a conceptual replication study with contrasting methodological decisions with the goal of producing similar results.

A group ICA-based data analysis paired with dual-regression was selected to search for rsfMRI connectivity between-group differences and additionally within-group differences relative to smelling scores. It is hypothesized that there will be significant differences in resting state networks between the healthy control group and PD group with severe hyposmia. An analysis of both subcortical and cortical brain volume morphometry was also performed with the intention of discovering brain volume discrepancies between groups. The hypothesis is that there will be significant cortical differences between groups, specifically the severely hyposmic PD group and controls. Hypothesized changes in subcortical volumes as well as overall specifically defined brain regions or networks affected by PD and hyposmia cannot be hypothesized due to lack of available and reliable published results.

# 2 Methods

## 2.1 Dataset

The dataset used for the present investigation was downloaded from a previous study published in 2018 by Yoneyama and colleagues. The data zip file was downloaded from a website called OpenNeuro.org (Access number: ds000245), and contained the structural and functional, raw fMRI data from 45

participants. Also provided in the file was a list of the participants' age, OSIT-J scores, ACE-R scores, and PD participants' respective disease duration time in months as well as their diagnosis age. The MRI scanning specifics were also made available and will be stated in the MRI acquisition section **2.1.4** on page 19.

### 2.1.1 Participants

The 45 (N = 45) included participants were recruited and scanned by researchers at the Nagoya University Department of Neurology. All participants were between the ages of 55-75 years old, 25 females and 20 males (female: n = 25; male: n = 20). All participants that reported having a history of other neurological/psychological diseases and/or a family history of Parkinsonism were excluded. To help minimize the potential for motion artifacts, tremor dominant PD patients as well as patients with focal deep white matter abnormalities, characterized by severe hyperintensities in the T2-weighted MRI images, were also excluded. The clinical PD participants were diagnosed after the age of 40 and diagnosed according the UK Brain Bank criteria; their disease progressions were categorized based on the Hoehn Yahr (HY) stages. Informed consent signed by all participants and ethical approval procedures were carried out by Yoneyama (2018) and colleagues in collaboration with the Nagoya University Graduate School of Medicine ethics committee. A table of participant's demographics is provided in *Appendix A*.

### 2.1.2 Neurocognitive Tests

All 45 participants were tested with the Odor Stick Identification Test for the Japanese (OSIT-J)(Kobayashi, 2015). This smell test is one comprised of 12 different odors that are familiar to Japanese people, and it is used clinically in Japan quite often. The smell is presented from a pen-like device and participants must select one of six possible answers; four main answers contain the one correct answer and the three other incorrect answers, and the last two possible answers are either that they do not know what they are smelling or that they cannot smell anything at all. Based on the final scores of the healthy controls (0-12 possible), all PD participants were categorized into two separate groups. The healthy control group had a mean OSIT-J score of

8.3/12 with a standard deviation (SD) of 2.2, which is within the normative range for the age group. PD patients with scores at least 1 SD below the control groups (>6/12) were categorized as having mild/moderate hyposmia (PD/MH) and patients scoring more than 2 SDs below the controls (>4/12) were categorized as having severe hyposmia (PD/SH). Scoring divided the PD patients into two groups of 15 people, coincidentally creating three equally sized groups: HC (n = 15), PD/MH (n = 15), and PD/SH (n = 15). It is important to note that the mean age between the HC group (M = 63.3 years, SD = 5.2 years) and PD/SH group (M = 70.7 years, SD = 4.8 years) differs significantly ($p < .001$) (Yoneyama et al., 2018).

All participants were also tested for potential cognitive impairments with the Addenbrooke's Cognitive Examination Revised (ACE-R). The ACE-R is a test battery for evaluation of cognition within five different categories: orientation and attention, memory, verbal fluency, language, and visuospatial ability. The ACE-R has an overall maximum score of 100, and the test also provides a Mini Mental State Exam (MMSE) score (0-30 possible). All participants scoring below or equal to 88 on the ACE-R were considered to have some cognitive impairment, and therefore were excluded from the study (Yoneyama et al. 2018).

### 2.1.3 PD Evaluations

Prior to Neurocognitive testing, all PD participants were thoroughly examined and categorized. The stage of the disease progression for each patient was calculated utilizing the modified Hoehn and Yahr scale containing stages 0-5 (modified version contains additional stages 1.5 and 2.5). All patients included in the present study were between stages 1 and 3, most were in stage 2 (M = 2.0). Whether or not PD patients' disease manifestations were right side dominant, left side dominant or bilateral was also recorded. Every PD patient was on medication, and a calculated Levadopa Equivalent Daily Dose (LEDD) score is provided. Finally, all PD patients were evaluated and scored with the Movement Disorder Society-Sponsored Revision of the Unified Parkinson's Disease Rating Scale (MDSUPDRS) parts one through four. Part one rates non-motor symptoms in everyday life, part two rates motor symptoms in everyday

life, part three scores a motor examination, and part four rates motor complications on a 0 – 4 scale. PD patients who reported experiencing hallucinations, anxiety, depression, dopamine dysregulation syndrome, apathy, and/or psychotic behaviors were also excluded (Yoneyma et al. 2018).

#### 2.1.4 MRI Data Acquisition

All MRI scans were acquired at the Nagoya University, Brain and Mind Research Center with a Siemens Magnetom Verio 3.0 Tesla scanner. A 34-channel head coil was used, and PD patients scanned "ON" medication. The scan specifics are as follows: "T1-weighted images (repetition time [TR] = 2.5 s, echo time [TE] = 2.48 ms, 192 sagittal slices with 1-mm thickness, field of view [FOV] = 256 mm, 256 × 256 matrix size) were acquired for anatomical reference. Total scanning time for the T1-weighted images was 349 seconds. rsfMRI scans (8 min, eyes closed) were also acquired (TR = 2.5 s, TE = 30 ms, 39 transverse slices with a 0.5-mm inter-slice interval and 3-mm thickness, FOV = 192 mm, 64 × 64 matrix dimension, flip angle = 80 degrees)" (Yoneyama et al., 2018, pp. 4).

### 2.2 Resting-State Analysis

#### 2.2.1 Preprocessing

Before preprocessing, the brain images of each subject were visually inspected for potential problems or artifacts. The raw T1-weighted images were then preprocessed initially with FMRIB's Software Library (FSL, version 5.09) (FMRIB's Software Library, Oxford, UK; Smith et al., 2004) anatomical preprocessing script, fsl_anat. This script runs the images through its standard preprocessing pipeline of reorientation to the MNI152 template (Evans et al., 1993), cropping, bias field correction, registration, brain extraction, tissue segmentation, and subcortical structure segmentation. However, a follow-up visual inspection of the output preprocessed anatomical brain images revealed obvious technical issues with the brain extraction step, which uses brightness values to discriminate the skull from the brain, and then remove the skull and everything outside of it from the image. The threshold determining which tissues are classified as brain matter or skull was then altered several times, with only slight improvements. Therefore, the anatomical preprocessing was

redone using the Advanced Normalization Tools Software package (ANTs) (Avants et al., 2011), which has very different methods of brain extraction, registration, and segmentation. The brain extraction is done by using a hybrid segmentation/template-based strategy, and the ANTs compatible T1-template selected was the available OASIS brain template created from a sample of adults with a wider range of age (Avants et al., 2010). The resulting output preprocessed T1-weighted images were much more accurately extracted and usable, in contrast.

T2-weighted BOLD functional images were preprocessed using FSLs FEAT (FMRI Expert Analysis Tool, FMRIB's Software Library, Oxford, UK; Smith et al., 2004; Jenkinson et al. 2012). The first four volumes were removed to correct for artifacts relative to the time in which the MRI scanner's magnetic field reaches equilibrium. The BOLD images from each subject were then motion corrected with MCFLIRT (Jenkinson et al., 2001;2002) and brain extracted was completed with BET. A spatial smoothing with a 6 mm Gaussian kernel (FWHM) was applied and the images were then registered with their corresponding structural images produced by ANTs. Both structural and functional images were normalized to the MNI152 standard space with an isotropic voxel resolution of approximately 2 x 2 x 2 cubic mm. The high-pass filter was not used, to prepare for the following noise reduction.

### 2.2.2 ICA-AROMA

To prepare for the ICA-based group analysis, the preprocessed T2 scans underwent an individual ICA-based stochastic noise reduction strategy called ICA-AROMA (ICA-based Automatic Removal of Motion Artifacts; Pruim et al., 2015). This robust, FSL compatible, nonparametric method statistically divides BOLD data into independent and spatially structured components. These components can then be categorized as "real" activation components reflective of a BOLD signal influx or conversely noise components reflective of biological or hardware related artifacts. The resulting ICA-AROMA spatial map components and accompanying frequency spectra values were first checked for quality, and then the automatically and corrected (denoised) output images were deemed suitable for the following analysis. ICA-AROMA's

automated classification system works by employing dual-regression and regressing out the noise components, the corrected data used in the group analysis were corrected non-aggressively. This nonaggressive categorization means the algorithm only removes components uniquely uncorrelated with obvious BOLD activity components. Conversely, strict aggressive regression techniques remove all components with unexplained variance even if some of the variance is shared with the real signal components (Prium et al. 2015).

The advantage to using this ICA-AROMA is mainly that it is an extremely data-driven method that requires no prior hypotheses about what constitutes noise artifacts. This method simply analyzes brain signals in their entirety at every voxel, and then provides a clear categorization of these signals. The other benefit to this method is that it preserves the temporal characteristics and degrees of freedom (tDoF) in the data. This consequently improves the statistical power of further comparisons, as well as overall reproducibility. ICA-AROMA has been evaluated in comparison to other "denoising" techniques, such as motion scrubbing, nuisance regression with 6 or 24 motion parameters, spike regression, and ICA-FIX. The ICA-AROMA method has consistently been reported to perform very accurately in comparison. ICA-AROMA also doesn't require a retraining-classifier like the alternative ICA-FIX (Salimi-Khorshidi et al., 2014; Graffanti et al., 2014) method (Pruim et al., 2015).

### 2.2.3 GICA and Dual-Regression

FSL's MELODIC (Multivariate Exploratory Linear Optimized Decomposition into Independent Components, FMRIB's Software Library, Oxford, UK) function decomposes the noise-corrected BOLD images from each individual subject, temporally concatenates them, analyzes the temporal and spatial patterns of activation signals, and finally separates these patterns into statistically independent components reflective of the entire or partial canonical resting state networks. The dimensions, or number of output components, can be either automatically generated or set prior. A standard image for normalization can be either a standard template, such as one generated using the MNI, or a template created from the participants' data. For the present study, a template for the GICA was generated using the data from the 15 HCs. This

template created in MELODIC was also 2 x 2 x 2 cubic mm in resolution with 12 DoF. The ICA analysis was run twice, both with 20 and 30 components to examine the differences in resulting interpretability of resting-state networks relative to the dimensionality choices. 20 – 30 components are highly recommended as the proper dimensionality for the model to be an optimal fit. Functional images were high pass-filtered with a cutoff value of 150 seconds (0.007 Hz), each subject's functional data was registered to their corresponding structural images and normalized to the HC template created. Time courses were also variance-normalized (Bijsterbosch et al., 2017; FMRIB's Software Library, Oxford, UK).

For the 20 and 30 component ICA results, dual-regression was applied using a simple dual-regression shell script and group comparison contrast files created in FSL's GLM setup. Dual-regression analysis of the ICA components operates, and outputs results in three stages: the first stage finds and outputs the subject-specific time courses using group-ICA spatial maps. The second locates subject-specific spatial maps using the time courses from stage one. Finally, the third stage performs a group analysis using the stage two spatial maps together with contrast files. The permutation number to correct for multiple comparisons was set to 5000 and the statistical values were calculated with an FSL function, *randomize* (Winkler et al., 2014), which employs a useful cluster-wise threshold enhancement technique (TFCE) (Smith & Nichols, 2009).

The main design files and contrasts were set up to run an ANOVA statistically comparing the components of all three groups, and three additional design files were created with age, smelling scores, and cognition scores as additional regressors (ANCOVA). No significant effects within-groups could be observed as a result of the covariate age; therefore, the effects of age were not regressed out. The final output was both 20 and 30 component statistical maps containing clusters of activation differences between the three groups, every component and accompanying significance values. Artifact components not reflective of interpretable brain activity were manually identified and removed from further interpretation. The concept of this group ICA in combination with dual-regression can be visualized in *figure 3.*

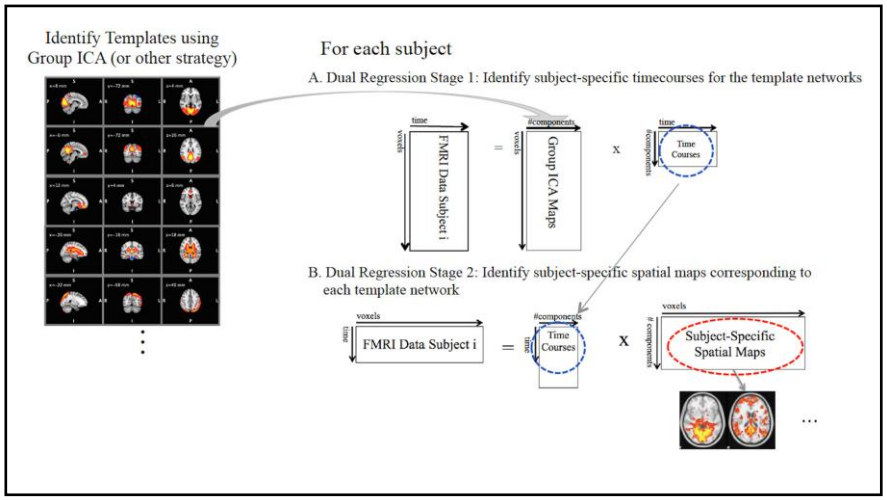


*Figure 3:* Group ICA (Nickerson et al., 2017)

Dual-regression paired with the ICA-based analysis produces a method that has consistently performed well in comparison to other techniques for resting-state network comparison. The advantage to this method is that it is data-driven, thus requiring no hypotheses or regions of interest selected beforehand like in seed-based rsfMRI methods. Every voxel is analyzed and there is a diminished potential of missing a significant difference in BOLD signal between subjects or groups. Alternative ICA-based methods commonly utilize "back-projection" for between subject statistical maps. The multiple linear regression approach presented here "estimates spatial and temporal dynamics at the subject level based on regression against the original data rather than estimating subject-specific maps by means of 'back-projection'. In the back-projection approach the estimated spatial maps necessarily lie within the space defined by (the pseudoinverse of) the initial subject-specific major Eigenspaces (PCA). As such, the final between-subject comparison (e.g. inference on the between-group difference) becomes dependent on the initial subject-specific reduction stages." (Beckmann et al., 2009, pp. 1). This alternative method is quite efficient, in terms of computation, but the statistical comparison interpreted from these back-projection maps tend to present a lot of Type one and two errors (Beckmann et al. 2009, Zuo et al., 2010). Nickerson et al. (2017) provides a comprehensive explanation and evaluation of this group

ICA-dual-regression (GICA-DR) approach, and also reports that this method is excellent in terms of validity, reliability, and overall reproducibility.

## 2.3 Brain Morphometry

Both cortical thickness values and subcortical brain tissue volumes were extracted with the popular automated Freesurfer software (Martinos Imaging Centre). Freesurfer requires no prior preprocessing and works automatically by: removing all non-brain tissue using a "hybrid watershed algorithm" (Segonne et al., 2004), a custom bias field correction, transforming the images to the Talairach standardized brain (Lancaster et al., 200), segmenting most visual brain structures, preforming an intensity normalization, aligning and parcellating images based on cortical folding patterns (Desikan et al., 2006; Fischl et al., 2004), estimating architectonic boundaries from training data, mapping cortical thickness/volume/surface area measures, and constructing surface models of the cerebrum one hemisphere at a time (Fischl & Dale, 2000). For all 45 subjects, a directory containing all T1-weighted structural images was input with a script, and automatically processed by Freesurfer.

The following comparison of cortical gray matter median thickness values and median subcortical structure volumes was independently conducted. The cortical regions and their accompanying labels were parcellated based on the Destrieux et al. (2010) atlas. The cortical atlas is based on a parcellation scheme that essentially divides the cortex based on patterns of cortical folding. The gyri and sulci are categorized by a curvature value threshold, with a gyrus including cortex visible on the pial surface and a sulcus is marked as nonvisible tissue (Fischl et al., 2004; Destrieux et al., 2010). The 40 subcortical regions were segmented and labeled with Freesurfer's automated Aseg atlas (Fischl et al., 2002). Both the median values for the subcortical volume as well as median thickness values of the cortex were extracted into a table. From the 40 subcortical regions the ventricles, CSF, white matter, brain stem, etc. values were deleted from further analysis. The remaining 32 subcortical volumes for each participant were analyzed in SPSS version 25.0 for Macintosh (IMB Corp.), where they were determined to be abnormally distributed; therefore, a Kruskal-Wallis nonparametric *H*-test was performed. The 72 median cortical

thickness values for each hemisphere were also compared in SPSS; however, the values were more normally distributed. Therefore, between groups comparisons were made with an ANCOVA.

# 3 Results

## 3.1 GICA – Dual-Regression Results

The ICA-based group analysis was run with 20 and 30, *figure 4* is an

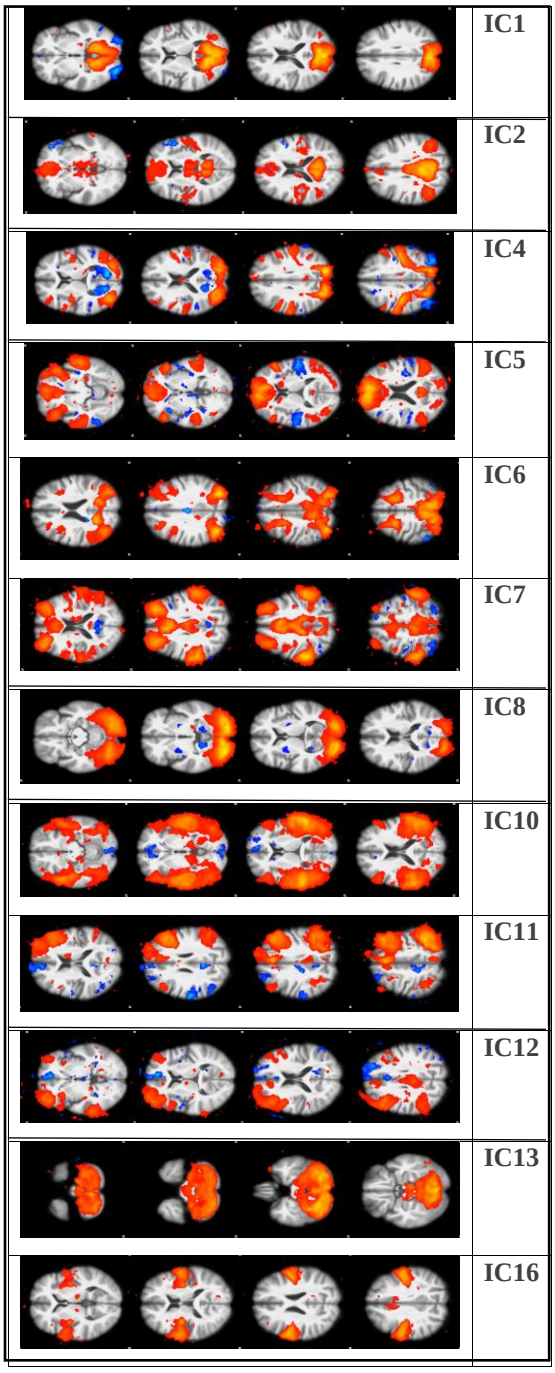


*Figure 4*: the spatial images to the left are the output independent components (IC) from the initial ICA analysis, after the denoising and before dual-regression. These are 12 of the 20 total components, 8 components were removed and considered to be artifact components. The 4 brain images selected for each component were chosen because they provide the best spatial interpretability. The horizontal plane image sequences go dorsally; from the bottom of the brain (left) to the top (right). The left hemisphere is pictured on the top part on the images, right hemisphere on the bottom. These images provide an insight into the robust gICA method for resting state analysis. This data-driven method is exploratory, and all components were generated based on temporal and spatial patterns within the dataset.

image of 12 out of the 20 ICs that were deemed representative of partial or complete canonical resting state networks, and the remaining eight artifact components were excluded. The dual-regression comparison of components between all three groups (ANOVA) yielded no significant differences in the IC networks. The same analysis was completed two additional times with each individual's smelling scores and ACE-R overall cognition scores as regressors, the resulting differentiating clusters were also nonsignificant.

The same ANOVA was completed on the second ICA-output with 30 components, 16 of which were considered to be "real" BOLD activation components (*figure 5*). The group comparison revealed a cluster of activation in

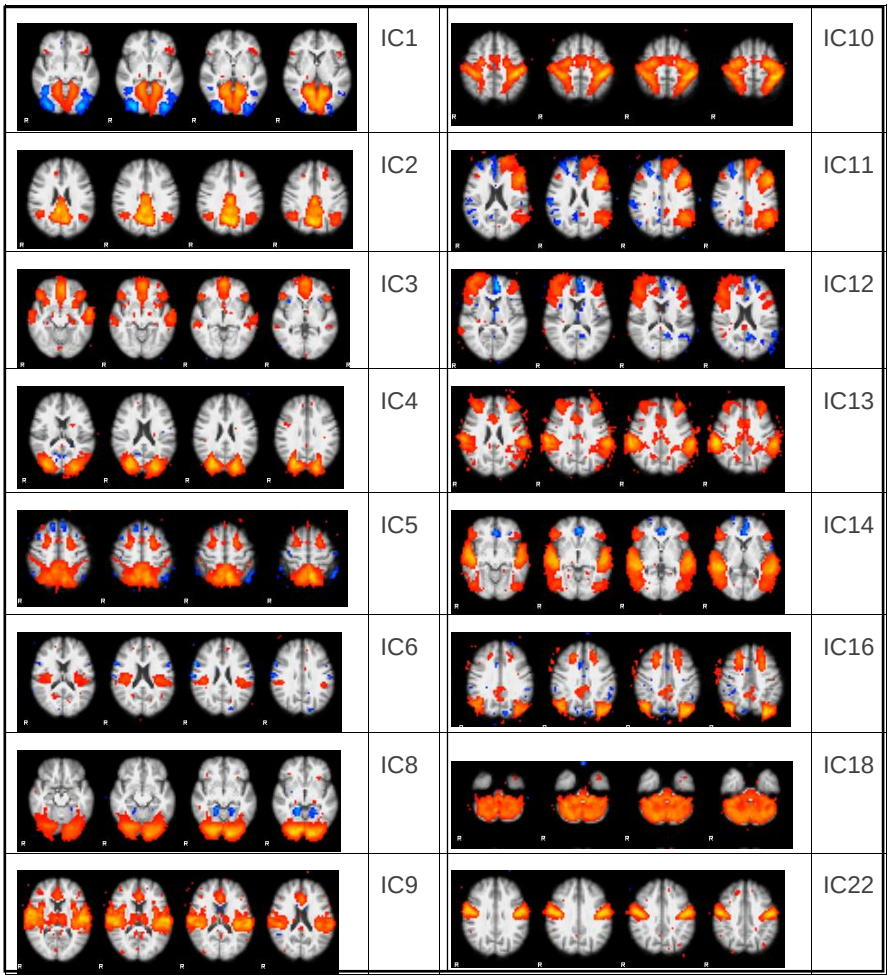


*Figure 5*: Above are the spatial maps of the 16 ICs selected from the 30 ICs, rather than 20. Some ICs look identical to the ICs in *Figure 4*, while some IC maps seem to be less interpretable and split. For example, IC8 in *Figure 4* seems to be a combination of IC9 and IC22 in this figure. These images were produced before the dual-regression analysis and do not represent changes between groups. The 4 images per IC are going ventrally in this figure (top to bottom), and the images are mirrored with the right hemisphere visualized on the left side.

the cerebellar component, more activated within the control group than the PD/SD ($p = 0.019$). This cluster was relatively small, made up of approximately 176 voxels. In addition, applying a Bonferroni correction for multiple comparisons (0.05/# of usable components) would set the significance threshold to $p < 0.003$. Therefore, this result is not considered significant. The smelling scores and cognition scores were also added as additional regressors in the group comparison, once again with no significant findings.

### 3.2 Subcortical Volume Results

A nonparametric, independent-samples Kruskal-Wallis *H*-test was performed in SPSS (IBM Corp.; version 25.0) to find significant group effects in the medium volumes of 16 subcortical segments in each hemisphere. No significant differences can be reported. The 32 overall subcortical regions, separated by hemisphere, and their corresponding p-values, ranging from $p < 0.073 – 0.915$ are available in *Appendix B*.

### 3.3 Cortical Thickness Results

Median thickness values calculated for all participants by Freesurfer, across all cortical regions were automatically parcellated utilizing the Destrieux Atlas (Destrieux et al., 2010). These values were then analyzed in SPSS version 25.0 (IMB Corp.) and were determined to be normally distributed ($p = 0.003$). Therefore, an ANCOVA was selected to identify the potential group effect with total intercranial volume and age as regressors of no interest. The results of the ANCOVA produced no significant findings comparing HCs, PD/MHs, and PD/SHs.

## 4 Discussion

### 4.1 Summary of Results

There were no significant results observed in the comparison of canonical resting state networks between the HC group, PD/MH group, and PD/SH group. There were also no reportable differences in subcortical brain

volume in 32 predefined structures as a result of PD or hyposmia. Nor were there significant changes in cortical thickness between groups.

### 4.2 Preservation of RSNs

The results support the null hypothesis, that PD patients on Levedopa have relatively preserved resting-state networks completely independent of the non-motor symptom hyposmia. There are very few studies reporting a severe change in the FC of PD patients in the "on" medication state (Yoneyama et al. 2018). The contradictory result of significantly unaltered resting connectivity in earlier-stage PD patients on medication is one that has been more often reported. Baggio and colleagues released a study this year (2019) comparing resting-state networks of PD patients on medication, MS patients on medication, and healthy controls with almost the exact same ICA and dual-regression methods in the present study. Their findings were the same: they only reported significant resting-state network alterations in the cerebellar component between PD patients and MS patients, and none between the PD patients and the healthy control group (Baggio et al., 2019).

Baggio et al. also released a study in 2015 comparing PD patients on medication with and without measurable cognitive decline to healthy controls using the same methodology, and only found significant resting-state network changes correlated with cognitive decline; not PD pathology. Bell et al. (2015) also report a medication induced preservation of brain connectivity when comparing PD patients both on and off their Levedopa medicine with HC. Therefore, the strong assumption can be made that the absence of significant differences in FC between PD patients and controls in the present study is a direct consequence of the PD patients being scanned on medication (Baggio et al., 2015;2019 & Bell et al. 2015).

### 4.3 GICA-DR Methodology

The completely conflicting results of the ICA/dual-regression analysis presented here, in comparison to Yoneyama et al.'s 2019 published results, illuminate a widespread issue in fMRI research. fMRI study results are often unreproducible even with the exact same data set and similar methodology. This study was a conceptual replication; therefore, methodological choices must

be compared and rightfully criticized. To begin, Yoneyama and colleagues regressed out effects of age and gender, using the data from the HC, before each analysis was ever performed. This was a rather unnecessary step, because in the present analysis the GICA-DR was completed with age as a regressor only to discover that age had no significant effect on FC. Regressing out variables prior to normalization that don't have an obvious and measurable effect on the data is not recommended because it could unnecessarily disrupt the data, potentially causing more type 1 errors (Pain et al. 2018).

The next methodological limitation in the Yoneyame et al. (2018) study was that they preprocessed their anatomical images using FSL FEAT (FMRIB's Software Library, Oxford, UK; Smith et al., 2004; Jenkinson et al. 2012), which of course included the BET brain extraction function. This is problematic, because when this same preprocessing step was performed in the current study the resulting T1- weighted images were extracted incorrectly and not in anyway usable. This resulted in the switch to ANTs (Avants et al., 2010) for structural image preprocessing and brain extraction. The following image in *Figure 6* shows the difference in performance between FSL's BET brain extraction and ANTs in one of the healthy control subjects.

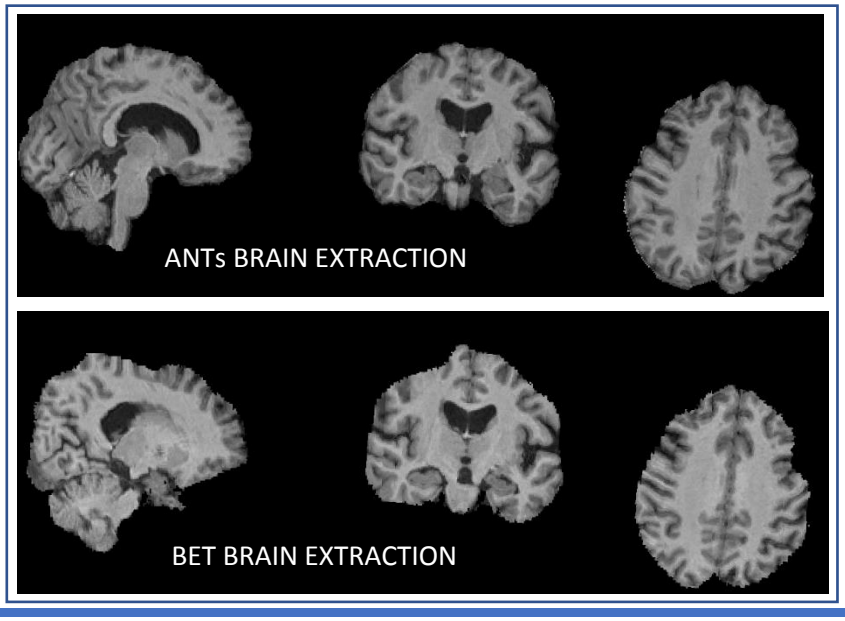


*Figure 6:* Above are two examples of structural T1-weighted brain images, preprocessed and extracted with two different software packages and skull stripping methods. The images are from the same subject (HC 6). The ANTs brain extraction default settings outperformed FSL's BET tool default settings.

It is unclear whether or not the researchers in the previous study used the default settings for the brain extraction, which produced the result pictured below. It is also not known why FSL's normally very accurate program performed so poorly on this dataset.

The remaining choices in methodology that differ between the current investigation and the prior will not be criticized, only stated. The denoising technique chosen by Yoneyama et al. (2018) was a nuisance regression of brain signals correlated with head motion, as well as the mean and temporally shifted signals from the CSF and white matter. This method is relatively good; however, ICA-based noise reduction methods have been reportedly more accurate and reproducible due to their data-driven complexity (Prium et al., 2015; Carone et al. 2017). The final GICA-DR analysis performed was essentially the same, except Yoneyama and researchers (2018) used the MNI standard brain template as opposed to a custom one, and they only ran the analysis with 30 components. Therefore, it can be reasonably inferred that the drastic differences in FC results are due to differences in preprocessing, denoising methods, and/or the choice to use a custom ICA-based templated for the dual-regression rather than a standard one.

One limitation to GICA itself, is that the selection of components is typically done manually, which leaves room for human error. Most of the components and their respective time-frequency spectra were rather easy to interpret, but there were still a few components that were more difficult to categorize. GICA also presents another reproducibility issue, and it is apparent when the same analysis is run more than once. Each run through of the GICA (as well as the single subject ICA denoising) produces components in a different order and maybe even slightly varied. These variances may be slight, but it is not feasible to ever expect the same exact output component. Nonetheless, the trade-off is that this method is completely exploratory and requires no prior assumptions about the temporal/spatial patterns or RSNs (Bijsterbosch et al. 2017). One additional limitation to the present GICA analysis would be that the GICA template for the dual-regression analysis was created with the HC group, and this is not recommended. This decision was made with the assumption that RSNs probably don't differ too much between

subjects, but it still may have caused some statistical biases. ICA-based analysis methods also tend to perform poorer on small sample sizes and noisy data (Bijsterbosch et al., 2017). The number of participants in the present study isn't too small, but the data quality for some subjects was rather noisy.

### 4.4 Preservation of Brain Structure

No statistically significant changes in subcortical or cortical regions consequent of PD or hyposmia can be reported. Brain atrophy observations play a notable role in the detection of disease or disease progression. A few studies report being able to use brain morphometry techniques to accurately discriminate between PD patients without dementia or other non-motor symptoms and HCs (Adeli et al., 2016; Bowman et al., 2016; Peng et al., 2017; & Nemmi et al., 2019). Though, most brain morphometry research only suggests atrophic changes in brain matter relative to PD with other non-motor symptoms, such as: dementia (Pan et al., 2013), visual-hallucinations (Ibarretxe-Bilbao et al., 2010), or depression (Kostic et al., 2010). Wattendorf et al. (2009) even reported significant differences in brain volume in both the piriform cortex and amygdala in PD patients with hyposmia.

On the other hand, there are a multitude of studies reporting the opposite, and stating that atrophic changes in brain volume or cortical thickness in cognitively normal PD patients are incredibly subtle and nearly impossible to image in the early stages (Messina et al., 2011; Peran et al., 2018; Pitcher et al., 2012). Messina and colleagues, for example, observed the brain's volumetric characteristics in HCs, progressive supranuclear palsy patients, multiple system atrophy patients, and PD patients. The researchers only reported significant differences in volume between the PD group and other clinical groups, and PD brains were indistinguishable from the brains imaged from the HC group. In addition, a meta-analysis of techniques to image PD pointed out that: "Atrophy ultimately occurs in PD; however, in previous studies of those with mild PD it is rather controversial as to whether there is atrophy, no change or an increase in brain volume." (Tuite, 2017, pp. 2). Therefore, it is assumed that the findings in this present study highlights the controversy of whether or not it's possible to use structural brain images and morphometry to consistently discriminate

between mild PD patients categorized as cognitively normal and healthy controls.

### 4.5 Freesurfer Methodology

Yoneyama and colleagues reported a number of gray matter volume changes in the PD/SH group compared to HC, and the present study reports none. Yoneyama et al. performed their voxel-based gray matter volume analysis manually with SPM. Freesurfer (Martinos Imaging Centre) automatically produced the cortical thickness values and subcortical volumes for all participants in this current study, and it has even been reported that Freesurfer performs very similarly to manual voxel-based methods in clinical populations (Lehmann et al., 2009). So, the inability to reproduce these results is somewhat puzzling. An assumption can be made that the Yoneyama et al. researchers regressed out effects of age and gender before the analysis, and that step was skipped in this study. Another limitation in the present study is that the images and values produced by Freesurfer were completely automated, and it would have been preferable and wise to apply a quality control on the data to correct for any problems.

Another potential reason for the lack of several morphological changes might be that Freesurfer performed poorer due to the asian ethnicity of the participants and their statistically different volumes, thicknesses, and surface areas in comparison to Caucasian brains (Chee et al., 2011; Tang et al., 2018). Tang et al. (2018) have reported several reproducible differences in brain structure between Chinese (East Asian) brains and Caucasian brains in all four lobes. The commonly used brain templates and automated software pipelines, including Freesurfer, were contracted from mostly western brains. To the best of my knowledge, it has not been proven that these atlases or software packages perform worse on brains of different ethnicities, however it is a reasonable speculation considering corrections are often made based on age and gender differences. A more likely explanation that may have caused a null finding, would be that the images had too many artifacts for Freesurfer's automated preprocessing to overcome. The raw data in this study was observed, and once

again in some participants the data was relatively noisy (Martinos Imaging Centre).

## 4.5 Conclusion

The results of this study were in no way as groundbreaking or significant as the results published by Yoneyama et al. (2018). Methodology changes with the same dataset should have, supposedly, reproduced slightly altered results, but alternatively the significant results were nonexistent. This is not an issue to take lightly, because it is unfortunately very reflective of the common credibility criticisms that exist within fMRI research. Credible results should in turn be reproducible, but with the increasing number of analysis pipelines and method techniques there are more opportunities to find a desired result rather than a valid one. Fortunately, Yoneyama and research associates are responsible for this current study existing by their decision to make their data public, which should be applauded. This is one way that the fields of cognitive neuroscience and psychology can evolve in terms of validity, along with researchers choosing to publish their analysis methods with excruciating detail. Another step in the right direction would be the development of standardized brain templates for an array of different ethnicities that are compatible with the major fMRI analysis software packages. Whether or not hyposmic related brain changes will be observed consistently enough with fMRI to serve as a biomarker for Parkinson's Disease or its pathological cognitive symptoms is a topic that requires further investigation. Nonetheless, advancements in technology and ethical good-practice shine hope for a better future of reproducible neuroscience and psychology research.

# References


Adeli, E., Shi, F., An, L., Wee, C. Y., Wu, G., Wang, T. & Shen, D. (2017). Joint feature-sample selection and robust diagnosis of Parkinson's disease from MRI data. *NeuroImage, 141*, 206-219. http://doi.org/10.1016/j.neuroimage.2016.05.054

Ashburner, J., & Friston, K. J. (2000). Voxel-based morphometry--the methods. *NeuroImage*, *11*(6 Pt 1), 805–821. https://doi.org/10.1006/nimg.2000.0582

Avants, B. B., Klein, A., Tustison, N. J.,Woo, J. & Gee, J.C. (2010). Evaluation of an open-access, automated brain extraction method on multi-site multi-disorder data. *Hum. Brain Mapp. Conf.*

Avants, B. B., Tustison, N. J., Song, G., Cook, P. A., Klein, A. & Gee, J. C. (2011). A reproducible evaluation of ANTs similarity metric performance in brain image registration. *Neuroimage, 54*(3), 2033-2044. http://doi.org/10.1016/j.neuroimage.2010.09.025

Baba, T., Takeda, A., Kikuchi, A., Nishio, Y., Hosokai, Y., Hirayama, K., ... Itoyama, Y. (2011). Association of olfactory dysfunction and brain. Metabolism in Parkinson's disease. *Movement Disorders: Official Journal of the Movement Disorder Society*, *26*(4), 621–628. https://doi.org/10.1002/mds.23602

Baggio, H. C., Segura, B. & Junque, C. (2015). Resting-state functional brain networks in Parkinson's disease. *CNS Neuroscience & Therapeutics, 21*, 793-801. https://doi.org/10.1111/cns.12417

Baggio, H. C., Abos, A. ,Segura, B. O., Campabadal, A., Uribe, C. O., Giraldo, D. M. , Perez-Soriano, A., Muñoz, E., Compta, Y., Junque, C. & Marti, M. J. (2019). Cerebellar resting-state functional connectivity in Parkinson's disease and multiple system atrophy: Characterization of abnormalities and potential for differential diagnosis at the single-patient level. *NeuroImage: Clinical, 22*. https://doi.org/10.1016/j.nicl.2019.101720

Beckmann, C. F., Mackay, C. E., Filippini, N. & Smith, S. M. (2009). Group comparison of resting-state FMRI data using multi-subject ICA and dual regression. NeuroImage, 47, 148. https://doi.org/10.1016/S1053-8119(09)71511-3

Bell, P. T., Gilat, M., O'Callaghan, C., Copland, D. A., Frank, M. J., Lewis, S. J. G. & Shine, J. M. (2015). Dopaminergic basis for impairments in functional connectivity across subdivisions of the striatum in Parkinson's disease. *Human Brain Mapping*, *36* (4), 1278-1291. https://doi.org/10.1002/hbm.22701

Bijsterbosch, J., Smith, S. M., & Beckmann, C. F. (2017). *Introduction to Resting State FMRI Functional Connectivity*. Oxford, United Kingdom: Oxford Press.

Bishop, D. (2019). Rein in the four horsemen of irreproducibility. *Nature, 568*, 435.

Bitter, T., Brüderle, J., Gudziol, H., Burmeister, H. P., Gaser, C. & Guntinas-Lichius, O. (2010). Gray and white matter reduction in hyposmic subjects — A voxel-

based morphometry study. *Brain Research, 1347*, 42-47. https://doi.org/10.1016/j.brainres.2010.06.003

Blumenfeld H.(2010) Limbic system: homeostasis, olfaction, memory, and emotion. *Neuroanatomy Through Clinical Cases*: *Sinauer Associates Incorporated*, 819-878.

Bohnen, N. I., Gedela, S., Herath, P., Constantine, G. M. & Moore, R. Y. (2008). Selective hyposmia in Parkinson disease. Association with hippocampal dopamine activity. *Neuroscience letters, 447*(1), 12–16. https://doi.org/10.1016/j.neulet.2008.09.070

Bowman, F. D., Drake, D. F. & Huddleston, D. E. (2016). Multimodal imaging signatures of Parkinson's disease. *Frontiers in Neuroscience, 10*(131). http://doi.org/10.3389/fnins.2016.00131

Cain, W. S., Gent, J. F., Goodspeed, R. B., & Leonard, G. (1988). Evaluation of olfactory dysfunction in the Connecticut Chemosensory Clinical Research Center (CCCRC). *Laryngoscope 98*, 83–88.

Carone, D., Licenik, R., Suri, S., Griffanti, L., Filippini, N. & Kennedy, J. (2017). Impact of automated ICA-based denoising of fMRI data in acute stroke patients. *Neuroimage Clinical, 16*, 23–31.

Chee, M. W. L., Zheng, H., Goh, J. O. S., Park, P. & Sutton, B. P. (2011). Brain structure in young and old east asians and westerners: comparisons of structural volume and cortical thickness. Journal of Cognitive Neuroscience, 23(5), 1065–1079. http://doi.org/10.1162/jocn.2010.21513

Clarkson, M. J., Cardoso, M. J., Ridgway, G. R., Modat, M., Leung, K. K., Rohrer, J. D., ... Ourselin, S. (2011). A comparison of voxel and surface based cortical thickness estimation methods. *NeuroImage, 57*(3), 856–865. https://doi.org/10.1016/j.neuroimage.2011.05.053

Cole, D. M., Smith, S. M., & Beckmann, C. F. (2010). Advances and pitfalls in the analysis and interpretation of resting-state FMRI data. *Frontiers in Systems Neuroscience, 4*(8), 1-15. https://doi.org/10.3389/fnsys.2010.00008

Desikan, R. S., Segonne, F., Fischl, B., Quinn, B. T., Dickerson, B. C., Blacker, D., Buckner, R.L., Dale, A. M., Maguire, R. P., Hyman, B. T., Albert, M. S. & Killany, R. J. (2006). An automated labeling system for subdividing the human cerebral cortex on MRI scans into gyral based regions of interest. *NeuroImage, 31*, 968-980.

Destrieux, C., Fischl, B. Dale, A. & Halgren, E. (2010). Automatic parcellation of human cortical gyri and sulci using standard anatomical nomenclature. *NeuroImage, 53*(1), 1-15. https://doi.org/10.1016/j.neuroimage.2010.06.010

Doty, R. L., Shaman, P., & Dann, M. (1984). Development of the University of Pennsylvania Smell Identification Test: A standardized microencapsulated test of olfactory function. *Physiology & Behavior (Monograph), 32*, 489-502.

Doty, R. L., Frye, R. E., & Agrawal, U. (1989). "Internal consistency reliability of the fractionated and whole University of Pennsylvania Smell Identification Test".

*Perception and Psychophysics*, *45*(5), 381–384. https://doi.org/10.3758/bf03210709

Doty, R.L. (2012). Olfaction in Parkinson's disease and related disorders. *Neurobiology of disease*, *46*(3), 527–552. https://doi.org/10.1016/j.nbd.2011.10.026

Double, K. L., Halliday, G. M., McRitchie, D. A., Reid, W. G. J., Hely, M. A. & Morris J. G. L. (1996). Regional brain atrophy in idiopathic Parkinson's disease and diffuse Lewy Body disease. *Dementia and Geriatric Cognitive Disorders*, *7*(6), 304-313.

Emamzadeh, F. N., & Surguchov, A. (2018). Parkinson's disease: biomarkers, treatment, and risk factors. *Frontiers in Neuroscience*, *12(612)*, 1-14. https://doi.org/10.3389/fnins.2018.00612

Esteban, O., Markiewicz, C. J., Blair, R. W., Moodie, C. A., Isik, A. I., Erramuzpe, A., ... Gorgolewski, K. J. (2019). fMRIPrep: A robust preprocessing pipeline for functional MRI. *Nature Methods*, *16*, 111–116. https://doi.org/10.1038/s41592-018-0235-4

Evans, A. C., Collins, D. L., Mills, S. R., Brown, E. D., Kelly, R. L. & Peters, T. M. (1993). 3D statistical neuroanatomical models from 305 MRI volumes. *Proc. IEEE-Nuclear Sci. Symp. Med. Imagine Conf.* 1813–1817.

Franks, K. H., Chuah, M. I., King, A. E., & Vickers, J. C. (2015). Connectivity of Pathology: The Olfactory System as a Model for Network-Driven Mechanisms of Alzheimer's Disease Pathogenesis. *Frontiers in Aging Neuroscience*, *7*, 234. https://doi.org/10.3389/fnagi.2015.00234

Firestein, S. (2001). How the olfactory system makes sense of scents. *Nature: Insight Review Articles 413*, 211-218.

Fischl, B. & Dale, A. M. (2000). Measuring the thickness of the human cerebral cortex from magnetic resonance images. *PNAS*, *97*(20), 11050-11055.

Fischl, B., Salat, D. H., Busa, E., Albert, M., Dieterich, M., Haselgrove, C., van der Kouwe, A., Killiany, R., Kennedy, D., Klaveness, S., Montillo, A., Makris, N., Rosen, B., Dale, A. M. (2002). Whole brain segmentation: automated labeling of neuroanatomical structures in the human brain. *Neuron 33*, 341-355.

Fischl, B., van der Kouwe, A., Destrieux, C., Halgren, E., Segonne, F., Salat, D. H., Busa, E., Seidman, L. J., Goldstein, J., Kennedy, D., Caviness, V., Makris, N., Rosen, B., Dale, A. M. (2004). Automatically parcellating the human cerebral cortex. *Cerebral Cortex 14*, 11-22.

Fischl, B. (2012). FreeSurfer. *NeuroImage*, *62*(2), 774–781. https://doi.org/10.1016/j.neuroimage.2012.01.021

Fjell, A. M, Walhovd, K. B., Reinvang, I., Lundervold, R., Salat, D., Quinn, B. T., Fischl, B. & Daled, A. M. (2006). Selective increase of cortical thickness in high-performing elderly—structural indices of optimal cognitive aging. *NeuroImage, 29*, 984-994. https://doi.org/10.1016/j.neuroimage.2005.08.007

Franks, K. H., Chuah, M. I., King, A. E., & Vickers, J. C. (2015). Connectivity of Pathology: The Olfactory System as a Model for Network-Driven Mechanisms

of Alzheimer's Disease Pathogenesis. *Frontiers in Aging Neuroscience*, *7*(234), 1-12. https://doi.org/10.3389/fnagi.2015.00234

Fullard, M. E., Tran, B., Xie, S. X., Toledo, J. B., Scordia, C., Linder, C., Purri, R., Weintraub, D., Duda, J. E., Chahine, L. M. & Morley, J. F. (2016). Olfactory impairment predicts cognitive decline in early Parkinson's disease. *Parkinsonism & Related Disorders, 25,* 45-51. https://doi.org/10.1016/j.parkreldis.2016.02.013

Gerrits, N. J.H. M., van Loenhoud, A. C., van den Berg, S. F., Berendse, H. W., Foncke, E. M. J, Klein, M., Stoffers, D., van der Werf, Y. D. & van den Heuvel, O. A. (2016). Cortical thickness, surface area and subcortical volume differentially contribute to cognitive heterogeneity in Parkinson's disease. *PLOS ONE, 11*(2). https://doi.org/10.1371/journal.pone.0148852

Ghahremani, M., Yoo, J., Chung, S. J., Yoo, K., Ye, J. C., & Jeong, Y. (2018). Alteration in the local and global functional connectivity of resting state networks in Parkinson's disease. *Journal of Movement Disorders*, *11*(1), 13–23. https://doi.org/10.14802/jmd.17061

Gibb, W. R. & Lees, A. J. (1988). The relevance of the Lewy body to the pathogenesis of idiopathic Parkinson's disease. *Journal of neurology, neurosurgery, and psychiatry, 51*(6), 745–752. https://doi.org/10.1136/jnnp.51.6.745

Giehl, K., Tahmasian, M., Eickhoff, S. B., & van Eimeren, T. (2019). Imaging executive functions in Parkinson's disease: An activation likelihood estimation meta-analysis. *Parkinsonism & Related Disorders.* Advance online publication. https://doi.org/10.1016/j.parkreldis.2019.02.015

Goebel, R. (2007). Localization of brain activity using functional magnetic resonance imaging. In C. Stippich (Ed.), *Clinical Functional MRI* (9 – 51). Springer Berlin, Heidelberg. Retrieved from https://doi.org/10.1007/978-3-540-49976-3_2

Goncalves, S. & Goldstein, B. J. (2016). Pathophysiology of olfactory disorders and potential treatment strategies. *Current Otorhinolaryngology Reports, 4(*2), 115-121. https://doi.org/10.1007/s40136-016-0113-5

Greve, D. N. (2011). An absolute beginner's guide to surface- and voxel-based morphometric analysis. *Intn. Soc. Mag. Reson. Med. Conf.*, 19

Griffanti, L., Salimi-Khorshidi, G., Beckmann, C. F., Auerbach, E. J., Douaud, D., Sexton, C. E., Zsoldos, E., Ebmeier, K., Filippini, N., Mackay, C. E., Moeller, S., Xu, J. G., Yacoub, E., Baselli, G., Ugurbil, K., Miller, K. L. & Smith, S. M. (2014). ICA-based artefact removal and accelerated fMRI acquisition for improved resting state network imaging. *NeuroImage*, *95*, 232-247.

Hubbard, P. S., Esiri, M. M., Reading, M., McShane, R. & Nagy, Z. (2007). Alpha-synuclein pathology in the olfactory pathways of dementia patients. *Journal of anatomy*, *211*(1), 117–124. https://doi.org/10.1111/j.1469-7580.2007.00748.x

Hummel, T., Sekinger, B., Wolf, S. R., Pauli, E., & Kobal, G. (1997). 'Sniffin' Sticks': olfactory performance assessed by the combined testing of odor identification, odor discrimination and olfactory threshold. *Chem Senses*, *22,* 39–51.

Hummel, T., Kobal, G., Gudziol, H., & Mackay-Sim, A. (2007). Normative data for the "Sniffin' Sticks" including tests of odor identification, odor discrimination, and olfactory thresholds: An upgrade based on a group of more than 3,000 subjects. *Eur Arch Otorhinolaryngol, 264*, 237–243. https://doi.org/10.1007/s00405-006-0173-0

Hummel, T., Fliessbach, K., Abele, M., Okulla, T., Reden, J., Reichmann, H., ... Haehner, A. (2010). Olfactory FMRI in patients with Parkinson's disease. *Frontiers in Integrative Neuroscience, 4*, 125. https://doi.org/10.3389/fnint.2010.00125

Ibarretxe-Bilbao, N., Ramirez-Ruiz, B., Carme, J., Marti, M. J., Valldeoriola, F., Bargallo, N., Juanes, S. & Tolosa, E. (2010). Differential progression of brain atrophy in Parkinson's disease with and without visual hallucinations. *Neurol Neurosurg Psychiatry, 81*, 650-657. http://doi.org/10.1136/jnnp.2009.179655

IBM Corp. Released 2017. IBM SPSS Statistics for Macintosh, Version 25.0. *Armonk, NY*: IBM Corp

Iijima, M., Kobayakawa, T., Saito, S., Osawa, M., Tsutsumi, Y., Hashimoto, S., & Iwata, M. (2008). Smell identification in Japanese Parkinson's disease patients: using the odor stick identification test for Japanese subjects. *Internal Medicine, 47*(21), 1887–1892. https://doi.org/10.2169/internalmedicine.47.1345

Jenkinson, M. & Smith, S. M. (2001). A global optimization method for robust affine registration of brain images. *Medical Image Analysis, 5*(2), 143-156.

Jenkinson, M., Bannister, P. R., Brady, J. M. & Smith, S. M. (2002). Improved optimization for the robust and accurate linear registration and motion correction of brain images. *NeuroImage, 17*(2), 825-841.

Jenkinson, M., Beckmann, C. F., Behrens, T. E. J., Woolrich, M. W., & Smith, S. M. (2012). FSL. *NeuroImage, 62*(2), 782–790. https://doi.org/10.1016/j.neuroimage.2011.09.015

Kim, J. K. (2019). Can olfactory tests help to diagnose Parkinson disease? *Clinical and Experimental Otorhinolaryngology*, *12*(2), 105–106. https://doi.org/10.21053/ceo.2019.00199

Kobal, G., Hummel, T., Sekinger, B., Barz, S., Roscher, S., & Wolf, S. (1996). "Sniffin' Sticks": screening of olfactory performance. *Rhinology 34*, 222–226.

Kobayashi, M. (2005). The Odor Stick Identification Test for the Japanese (OSIT-J): clinical suitability for patients suffering from olfactory disturbance. Chemical Senses, 31(1), 216-217. https://doi.org/10.1093/chemse/bjh191

Koch, W., Teipel, S., Mueller, S., Buerger, K., Bokde, A., Hampel, H., Coates, U., Reiser, M. & Meindl, T. (2010). Effects of aging on default mode network activity in resting state fMRI: Does the method of analysis matter? *NeuroImage, 51*(1), 280–287. https://doi.org/10.1016/j.neuroimage.2009.12.008

Kostić, V. S., Agosta, F., Petrović, I., Galantucci, S., Špica, V., Ječmenica-Lukic, M. & Filippi, M. (2010). Regional patterns of brain tissue loss associated with depression in Parkinson disease. *Journal of Neurology*, *75*(10), 857-863. http://doi.org/10.1212/WNL.0b013e3181f11c1d

Kurth, F., Luders, E., & Gaser, C. (2015). Voxel-based morphometry. *Brain Mapping: An Encyclopedic Reference, 1*, 345–349. https://doi.org/10.1016/B978-0-12-397025-1.00304-3

Lancaster, J. L., Woldorff, M.G., Parsons L. M., Liotti, M., Freitas, C. S., Rainey, L., Kochunov, P. V., Nickerson, D., Mikiten, S. A.& Fox, P. T. (2000) Automated Talairach atlas labels for functional brain mapping. *Human Brain Mapping, 10*, 120-131.

Lehmann, M., Douiri, A., Kim, L. G., Modat, M., Chan, D., Ourselin, S., Barnes, J. & Fox, N. C. (2010). Atrophy patterns in Alzheimer's disease and semantic dementia: A comparison of FreeSurfer and manual volumetric measurements. *NeuroImage, 49*(3), 2264-2274.

Messina, D., Cerasa, A., Condino, F., Arabia, G., Novellino, F., Nicoletti, G., Salsone, M., Morelli, M., Lanza, P. L. & Quattrone, A. (2011). Patterns of brain atrophy in Parkinson's disease, progressive supranuclear palsy and multiple system atrophy. Parkinsonism and Related Disorders 17, 172-176.

Morley, J. F., Weintraub, D., Mamikonyan, E., Moberg, P. J., Siderowf, A. D. & Duda, J. D. (2011). Olfactory dysfunction is associated with neuropsychiatric manifestations in Parkinson's disease. *Movement Disorders, 26*(11), 2051-2057. https://doi.org/10.1002/mds.23792

Morley, J. F., Cohen, A., Silveira-Moriyama, L., Lees, A. J., Williams, D. R., Katzenschlager, R., ... Duda, J. E. (2018). Optimizing olfactory testing for the diagnosis of Parkinson's disease: Item analysis of the university of Pennsylvania smell identification test. *NPJ Parkinson's Disease*, *4*(2), 1-7. https://doi.org/10.1038/s41531-017-0039-8

Murphy, C., Schubert, C. R., Cruickshanks, K. J., Klein, B. E., Klein, R., & Nondahl, D. M. (2002). Prevalence of olfactory impairment in older adults. *JAMA, 288*(18), 2307–2312.

Nemmi, F., Pavy-LeTraon, A., Phillips, O. R., Galitzky, M., Meissner, W. G., Rascol, O. & Péran, P. (2019). A totally data-driven whole-brain multimodal pipeline for the discrimination of Parkinson's disease, multiple system atrophy and healthy control. *NeuroImage: Clinical Volume*, 23. https://doi.org/10.1016/j.nicl.2019.101858

Nickerson, L. D., Smith, S. M., Öngür, D., & Beckmann, C. F. (2017). Using dual regression to investigate network shape and Amplitude in Functional Connectivity Analyses. *Frontiers in Neuroscience, 11*(115). https://doi.org/10.3389/fnins.2017.00115

Pan, P. L., Shi, H. C., Zhong, J. G., Xiao, P. R., Shen, Y., Wu, L. J. & Li, H. L. (2013). Gray matter atrophy in Parkinson's disease with dementia: evidence from meta-analysis of voxel-based morphometry studies. Neurol. Sci., 34(5), 613-619. doi:10.1007/s10072-012-1250-3

Pain, O., Dudbridge, F. & Ronald, A. (2018). Are your covariates under control? How normalization can re-introduce covariate effects. *European Journal of Human Genetics, 26*, 1194–1201.

Parkinson, J. (2002). An essay on the shaking palsy. *The Journal of Neuropsychiatry and Clinical Neurosciences, 14*(2), 223-236. (Original work published 1817).

Peng, B., Wang, S., Zhou, Z., Liu, Y., Tong, B., Zhang, T. & Dai, Y. (2017) A multilevel-ROI-features-based machine learning method for detection of morphometric biomarkers in Parkinson's disease. *Neuroscience Letters, 651*, 88-94.

Péran, P., Barbagallo, G., Nemmi, F., Sierra, M., Galitzky, M., Pavy- Le Traon, A., Payoux, P., Meissner, W. G. & Rascol, O. (2018). MRI supervised and unsupervised classification of Parkinson's disease and multiple system atrophy. Journal of Movement Disorders 33(4), 600-608. https://doi.org/10.1002/mds.27307

Pitcher, T. L., Melzer, T. R., MacAskill, M. R., Graham, C. F. Livingston, L., Keenan, R. J. & Anderson, T. J. (2012). Reduced striatal volumes in Parkinson's disease: a magnetic resonance imaging study. *Translational Neurodegeneration, 1*(1). https://doi.org/10.1186/2047-9158-1-17

Poldrack, R. A., Baker, C. I., Durnez, J., Gorgolewski, K. J., Matthews, P. M., Munafò, M. R., ... Yarkoni, T. (2017). Scanning the horizon: towards transparent and reproducible neuroimaging research. *Nature Reviews. Neuroscience, 18*(2), 115–126. https://doi.org/10.1038/nrn.2016.167

Ponsen, M. M., Stoffers, D., Booij, J., van Eck-Smit, B. L. F., Wolters, E. C., & Berendse, H. W. (2004). Idiopathic hyposmia as a preclinical sign of Parkinson's disease. *Annals of Neurology, 56*(2), 173 – 181. https://doi.org/10.1002/ana.20160

Postuma, R. B., Berg, D., Stern, M., Poewe, W., Olanow, C. W., Oertel, W., . . . Deuschl, G. (2015). MDS clinical diagnostic criteria for Parkinson's disease. *Movement Disorders: Official Journal of the Movement Disorder Society, 30*(12), 1591–1601. https://doi.org/10.1002/mds.26424

Pruim, R. H., Mennes, M., Buitelaar, J. K. & Beckmann, C. F. (2015). Evaluation of ICA-AROMA and alternative strategies for motion artifact removal in resting state fMRI. *Neuroimage, 112*, 278–287.

Radziunas, A., Deltuva, V. P., Tamasauskas, A., Gleizniene, R., Pranckeviciene, A., Petrikonis, K. & Bunevicius, A. (2018). Brain MRI morphometric analysis in Parkinson's disease patients with sleep disturbances. *BMC Neurology, 18*(88).

Righart, R., Schmidt, P., Dahnke, R., Biberacher, V., Beer, A., Buck, D., . . . Mühlau, M. (2017). Volume versus surface-based cortical thickness measurements: A comparative study with healthy controls and multiple sclerosis patients. *PloS One, 12*(7). https://doi.org/10.1371/journal.pone.0179590

Rodríguez-Violante, M., Gonzalez-Latapi, P., Camacho-Ordoñez, A.,Martínez-Ramírez, D., Morales-Briceño, H. & Cervantes-Arriaga, A. (2014). Low specificity and sensitivity of smell identification testing for the diagnosis

of Parkinson's disease. *Arq Neuropsiquiatr*, *72*(1), 33-37. https://doi.org/10.1590/0004-282X20130190

Roy, A. K., Shehzad, Z., Margulies, D. S., Kelly, A. M. C., Uddin, L. Q., Gotimer, K., ... Milham, M. P. (2009). Functional connectivity of the human amygdala using resting state fMRI. *NeuroImage*, *45*(2), 614–626. https://doi.org/10.1016/j.neuroimage.2008.11.030

Saito, Y., Shioya, A., Sano, T., Sumikura, H., Murata, M., & Murayama, S. (2016). Lewy body pathology involves the olfactory cells in Parkinson's disease and related disorders. *Movement Disorders: Official Journal of the Movement Disorder Society*, *31*(1), 135–138. https://doi.org/10.1002/mds.26463

Salimi-Khorshidi, G., Douaud, G., Beckmann, C. F., Glasser, M. F., Griffanti, L. & Smith, S.M. (2014). Automatic denoising of functional MRI data: combining independent component analysis and hierarchical fusion of classifiers. *NeuroImage*, *90*, 449-468.

Segonne, F., Dale, A. M., Busa, E., Glessner, M., Salat, D., Hahn, H. K. & Fischl, B. (2004). A hybrid approach to skull stripping problem in MRI. *Neuroimage*, *22*, 1060-1075.

Schapira, A. H. (2006). Etiology of Parkinson's disease. *Neurology*, *66*(10 suppl 4), 10-23. http://doi.org/10.1212/wnl.66.10_suppl_4.s10

Shi, L., Liang, P., Luo, Y., Liu, K., Mok, V. C. T., Chu, W. C. W., Wang, D., & Li, K. (2017). Using large-scale statistical Chinese brain template (Chinese 2020) in popular neuroimage analysis toolkits. *Frontiers in Human Neuroscience*, *11*(414). https://doi.org/10.3389/fnhum.2017.00414

Smith, S. M., Jenkinson, M., Woolrich, M. W., Beckmann, C. F., Behrens,

T. E., Johansen-Berg, H., ... Matthews, P. M. (2004). Advances in functional and structural MR image analysis and implementation as FSL. *NeuroImage*, *23*(1), 208–219. https://doi.org/10.1016/j.neuroimage.2004.07.051

Smith, S. M. & Nichols, T. E. (2009). Threshold-free cluster enhancement: addressing problems of smoothing, threshold dependence and localization in cluster inference. *NeuroImage*, *44*(1), 83-98.

Soares, J. M., Magalhães, R., Moreira, P. S., Sousa, A., Ganz, E., Sampaio, A., ... Sousa, N. (2016). A hitchhiker's guide to functional magnetic resonance imaging. *Frontiers in Neuroscience*, *10*(515). https://doi.org/10.3389/fnins.2016.00515

Sobel, N., Prabhakaran, V., Desmond, J. E., Glover, G. H., Goode, R. L., Sullivan, E. V., & Gabrieli, J. D. (1998). Sniffing and smelling: Separate subsystems in the human olfactory cortex. *Nature*, *392*(6673), 282–286. https://doi.org/10.1038/32654

Su, M., Wang, S., Fang, W., Zhu, Y., Li, R., Sheng, K., Zou, D., Han, Y., Wang, X. & Cheng, O. (2015). Alterations in the limbic/paralimbic cortices of

Parkinson's disease patients with hyposmia under resting-state functional MRI by regional homogeneity and functional connectivity analysis. *Parkinsonism & Related Disorders, 21*(7), 698-703. https://doi.org/10.1016/j.parkreldis.2015.04.006

Sveinbjornsdottir, S. (2016). The clinical symptoms of Parkinson's disease. *Journal of Neurochemistry, 139*(Suppl 1), 318–324. https://doi.org/10.1111/jnc.13691

Tang, Y., Zhao, L., Lou, Y., Shi, Y., Fang, R., Lin, X., Liu, S. & Toga, A. (2018). Brain structure differences between Chinese and Caucasian cohorts: A comprehensive morphometry study. *Hum Brain Mapp, 39*(5), 2147-2155. https://doi.org/10.1002/hbm.23994

Tucholka, A., Fritsch, V., Poline, J. B & Thirion, B. (2012). An empirical comparison of surface-based and volume-based group studies in neuroimaging. *NeuroImage, Elsevier*, *63*(3), 1443-1453. https://doi.org/10.1016/j.neuroimage.2012.06.019. hal-00723437v3

Tuite, P. (2017). Brain magnetic resonance Imaging (MRI) as a potential biomarker for Parkinson's disease (PD). Brain Sciences, 7(68). https://doi.org/10.3390/brainsci7060068

van Erp, T. G. M., Hibar, D. P., Rasmussen, J. M., Glahn, D. C., Pearlson, G. D., Andreassen, O. A., Agartz, I., Westlye, L. T., Haukvik, U. K., Dale, A. M., Melle, I., Hartberg, C.B., Gruber, O., … & Turner, J. A. (2016). Subcortical brain volume abnormalities in 2028 individuals with schizophrenia and 2540 healthy controls via the ENIGMA consortium. *Molecular Psychiatry, 21*, 547–553. https://doi.org/10.1038/mp.2015.63

Wattendorf, E., Welge-Lu¨ssen, A., Fiedler, K., Bilecen, D., Wolfensberger, M., Fuhr, P., Hummel, T. & Westermann, B. (2009). Olfactory impairment predicts brain atrophy in Parkinson's disease. *The Journal of Neuroscience, 29*(49), 15410 –15413.

Wen, M.-C., Xu, Z., Lu, Z., Chan, L. L., Tan, E. K., & Tan, L. C. S. (2017). Microstructural network alterations of olfactory dysfunction in newly diagnosed Parkinson's disease. *Nature: Scientific Reports, 7*(12559). https://doi.org/10.1038/s41598-017-12947-7

Westermann, B., Wattendorf, E., Schwerdtfeger, U., Husner, A., Fuhr, P., Gratzl, O., Hummel, T., Bilecen, D. & Welge-Lüssen, A. (2008). Functional imaging of the cerebral olfactory system in patients with Parkinson's disease. *Neurology, Neurosurgery, & Psychiatry, 79*(1). http://dx.doi.org/10.1136/jnnp.2006.113860

Winkler, A. M., Ridgway, G. R., Webster, M. A., Smith, S. M. & Nichols, T. E. (2014). Permutation inference for the general linear model. *NeuroImage, 92*, 381-397.

Witt, M., Bormann, K., Gudziol, V., Pehlke, K., Barth, K., Minovi, A., ... Hummel, T. (2009). Biopsies of olfactory epithelium in patients with Parkinson's disease. *Movement Disorders: Official Journal of the*

*Movement Disorder Society*, *24*(6), 906–914. https://doi.org/10.1002/mds.22464

Wu, T., Wang, L., Chen, Y., Zhao, C., Li, K., & Chan, P. (2009). Changes of functional connectivity of the motor network in the resting state in Parkinson's disease. *Neuroscience Letters*, *460*(1), 6–10. https://doi.org/10.1016/j.neulet.2009.05.046

Yeo, B. T. T., Krienen, F. M., Sepulcre, J., Sabuncu, M. R., Lashkari, D., Hollinshead, M., ... Buckner, R. L. (2011). The organization of the human cerebral cortex estimated by intrinsic functional connectivity. *Journal of Neurophysiology*, *106*(3), 1125–1165. https://doi.org/10.1152/jn.00338.2011

Yoneyama, N., Watanabe, H., Kawabata, K., Bagarinao, E., Hara, K., Tsuboi, T., ... Sobue, G. (2018). Severe hyposmia and aberrant functional connectivity in cognitively normal Parkinson's disease. *PloS One, 13*(1). https://doi.org/10.1371/journal.pone.0190072

Yoshida, H., Terada, S., Honda, H., Ata, T., Takeda, N., Kishimoto, Y., ... Kuroda, S. (2011). Validation of Addenbrooke's cognitive examination for detecting early dementia in a Japanese population. *Psychiatry Research, 185*(1-2), 211 – 214. https://doi.org/10.1016/j.psychres.2009.06.012

Yousem, D. M., Geckle, R. J., Bilker W., McKeown, D.A., & Doty, R. L. (1996). MR evaluation of patients with congenital hyposmia or anosmia. *AJR, 166*, 439–443. https://doi.org/93.132.103.142

Zald, D. H. & Pardo, J. V. (2000). Functional Neuroimaging of the Olfactory System in Humans. *International Journal of Psychophysiology, 36*, 165-181.

Zilles, K., Kawashima, R., Dabringhaus, A., Fukuda, H., & Schormann, T. (2001). Hemispheric shape of European and Japanese brains: 3-D MRI analysis of intersubject variability, ethnical, and gender differences. *NeuroImage*, *13*(2), 262 – 271. https://doi.org/10.1006/nimg.2000.0688

# Appendices

**Appendix A:** Participant Demographics (Yoneyama et al., 2018, table 1)

**Table 1. Patient demographics.**

| | PD with severe hyposmia | PD with no/mild hyposmia | Healthy controls | P values |
|---|---|---|---|---|
| Number | 15 | 15 | 15 | NS |
| Male/Female | 7/8 | 6/9 | 7/8 | NS |
| Age at examination | 70.7(4.8) | 64.4 (7.2) | 63.3(5.2) | $p = 0.01$ |
| Duration (y) | 5.9(3.7) | 6.1(3.2) | NA | NS |
| ACE-R | 94.3(3.4) | 96.1(3.1) | 97.3(2.9) | NS |
| MMSE | 29.1 (1.1) | 29.0 (1.3) | 29.5 (0.6) | NS |
| OSIT-J | 1.7(1.1) | 7.5(1.5) | 10.4 (1.3) | $p < 0.0001$ |
| Laterality (R/L/B) | 7/7/1 | 4/11/0 | NA | NS |
| LEDD | 455.9(377.8) | 394.7(277.0) | NA | NS |
| Hoehn and Yahr stages | 2.0(0.4) | 2.0(0.5) | NA | NS |
| MDSUPDRS-I | 5.1(4.2) | 4.6(3.9) | NA | NS |
| MDSUPDRS-II | 7.5(4.5) | 10.3(6.5) | NA | NS |
| MDSUPDRS-III | 19.3(7.9) | 21.2(9.4) | NA | NS |
| MDSUPDRS-IV | 1.9(3.5) | 2.0(3.3) | NA | NS |

Data are means ± standard deviation (SD). PD, Parkinson's disease; ACE-R, Addenbrooke's Cognitive Examination-Revised; MMSE, mini-mental state examination; R, right side predominant; L, left side predominant; B, bilateral; LEDD, levodopa equivalent dose; MDS-UPDRS, Movement Disorder Society-Sponsored Revision of the Unified Parkinson's Disease Rating Scale; NS, not significantly different; NA, not applicable.

Comparisons of the differences in gender and laterality were performed using the chi-square test. Hoehn and Yahr stages and the MDSUPDRS-IV scores were compared using the Student's t-test. To compare duration, MDSUPDRS-I/II/III scores and LEDD, we used the Mann- Whitney U test. To compare age at examination, MMSE and ACE-R, we used one-way analysis of variance. To evaluate differences in OSIT-J we used in the Kruskal-Wallis test.

**Appendix B:** Subcortical volumes; SPSS output

**Hypothesis Test Summary**

| | Null Hypothesis | Test | Sig. | Decision |
|---|---|---|---|---|
| 1 | The medians of Left-Thalamus-Proper are the same across categories of VAR00001. | Independent-Samples Median Test | .315 | Retain the null hypothesis. |
| 2 | The distribution of Left-Thalamus-Proper is the same across categories of VAR00001. | Independent-Samples Kruskal-Wallis Test | .467 | Retain the null hypothesis. |
| 3 | The medians of Left-Cerebellum-White-Matter are the same across categories of VAR00001. | Independent-Samples Median Test | .315 | Retain the null hypothesis. |
| 4 | The distribution of Left-Cerebellum-White-Matter is the same across categories of VAR00001. | Independent-Samples Kruskal-Wallis Test | .795 | Retain the null hypothesis. |
| 5 | The medians of Left-Cerebellum-Cortex are the same across categories of VAR00001. | Independent-Samples Median Test | .915 | Retain the null hypothesis. |
| 6 | The distribution of Left-Cerebellum-Cortex is the same across categories of VAR00001. | Independent-Samples Kruskal-Wallis Test | .920 | Retain the null hypothesis. |
| 7 | The medians of Left-Caudate are the same across categories of VAR00001. | Independent-Samples Median Test | .537 | Retain the null hypothesis. |
| 8 | The distribution of Left-Caudate is the same across categories of VAR00001. | Independent-Samples Kruskal-Wallis Test | .384 | Retain the null hypothesis. |
| 9 | The medians of Left-Putamen are the same across categories of VAR00001. | Independent-Samples Median Test | .315 | Retain the null hypothesis. |
| 10 | The distribution of Left-Putamen is the same across categories of VAR00001. | Independent-Samples Kruskal-Wallis Test | .116 | Retain the null hypothesis. |
| 11 | The medians of Left-Pallidum are the same across categories of VAR00001. | Independent-Samples Median Test | .701 | Retain the null hypothesis. |
| 12 | The distribution of Left-Pallidum is the same across categories of VAR00001. | Independent-Samples Kruskal-Wallis Test | .556 | Retain the null hypothesis. |
| 13 | The medians of Left-Hippocampus are the same across categories of VAR00001. | Independent-Samples Median Test | .315 | Retain the null hypothesis. |
| 14 | The distribution of Left-Hippocampus is the same across categories of VAR00001. | Independent-Samples Kruskal-Wallis Test | .181 | Retain the null hypothesis. |
| 15 | The medians of Left-Amygdala are the same across categories of VAR00001. | Independent-Samples Median Test | .701 | Retain the null hypothesis. |

Asymptotic significances are displayed. The significance level is .05.

**Hypothesis Test Summary**

| | Null Hypothesis | Test | Sig. | Decision |
|---|---|---|---|---|
| 16 | The distribution of Left-Amygdala is the same across categories of VAR00001. | Independent-Samples Kruskal-Wallis Test | .721 | Retain the null hypothesis. |
| 17 | The medians of Left-Accumbens-area are the same across categories of VAR00001. | Independent-Samples Median Test | .701 | Retain the null hypothesis. |
| 18 | The distribution of Left-Accumbens-area is the same across categories of VAR00001. | Independent-Samples Kruskal-Wallis Test | .454 | Retain the null hypothesis. |
| 19 | The medians of Left-VentralDC are the same across categories of VAR00001. | Independent-Samples Median Test | .915 | Retain the null hypothesis. |
| 20 | The distribution of Left-VentralDC is the same across categories of VAR00001. | Independent-Samples Kruskal-Wallis Test | .839 | Retain the null hypothesis. |
| 21 | The medians of Right-Cerebellum-White-Matter are the same across categories of VAR00001. | Independent-Samples Median Test | .701 | Retain the null hypothesis. |
| 22 | The distribution of Right-Cerebellum-White-Matter is the same across categories of VAR00001. | Independent-Samples Kruskal-Wallis Test | .763 | Retain the null hypothesis. |
| 23 | The medians of Right-Cerebellum-Cortex are the same across categories of VAR00001. | Independent-Samples Median Test | .701 | Retain the null hypothesis. |
| 24 | The distribution of Right-Cerebellum-Cortex is the same across categories of VAR00001. | Independent-Samples Kruskal-Wallis Test | .988 | Retain the null hypothesis. |
| 25 | The medians of Right-Thalamus-Proper are the same across categories of VAR00001. | Independent-Samples Median Test | .915 | Retain the null hypothesis. |
| 26 | The distribution of Right-Thalamus-Proper is the same across categories of VAR00001. | Independent-Samples Kruskal-Wallis Test | .387 | Retain the null hypothesis. |
| 27 | The medians of Right-Caudate are the same across categories of VAR00001. | Independent-Samples Median Test | .915 | Retain the null hypothesis. |
| 28 | The distribution of Right-Caudate is the same across categories of VAR00001. | Independent-Samples Kruskal-Wallis Test | .610 | Retain the null hypothesis. |

Asymptotic significances are displayed. The significance level is .05.

**Hypothesis Test Summary**

| | Null Hypothesis | Test | Sig. | Decision |
|---|---|---|---|---|
| 29 | The medians of Right-Putamen are the same across categories of VAR00001. | Independent-Samples Median Test | .185 | Retain the null hypothesis. |
| 30 | The distribution of Right-Putamen is the same across categories of VAR00001. | Independent-Samples Kruskal-Wallis Test | .073 | Retain the null hypothesis. |
| 31 | The medians of Right-Pallidum are the same across categories of VAR00001. | Independent-Samples Median Test | .315 | Retain the null hypothesis. |
| 32 | The distribution of Right-Pallidum is the same across categories of VAR00001. | Independent-Samples Kruskal-Wallis Test | .403 | Retain the null hypothesis. |
| 33 | The medians of Right-Hippocampus are the same across categories of VAR00001. | Independent-Samples Median Test | .915 | Retain the null hypothesis. |
| 34 | The distribution of Right-Hippocampus is the same across categories of VAR00001. | Independent-Samples Kruskal-Wallis Test | .553 | Retain the null hypothesis. |
| 35 | The medians of Right-Amygdala are the same across categories of VAR00001. | Independent-Samples Median Test | .915 | Retain the null hypothesis. |
| 36 | The distribution of Right-Amygdala is the same across categories of VAR00001. | Independent-Samples Kruskal-Wallis Test | .857 | Retain the null hypothesis. |
| 37 | The medians of Right-Accumbens-area are the same across categories of VAR00001. | Independent-Samples Median Test | .915 | Retain the null hypothesis. |
| 38 | The distribution of Right-Accumbens-area is the same across categories of VAR00001. | Independent-Samples Kruskal-Wallis Test | .876 | Retain the null hypothesis. |
| 39 | The medians of Right-VentralDC are the same across categories of VAR00001. | Independent-Samples Median Test | .241 | Retain the null hypothesis. |
| 40 | The distribution of Right-VentralDC is the same across categories of VAR00001. | Independent-Samples Kruskal-Wallis Test | .525 | Retain the null hypothesis. |
| 41 | The medians of CC_Posterior are the same across categories of VAR00001. | Independent-Samples Median Test | .185 | Retain the null hypothesis. |

Asymptotic significances are displayed. The significance level is .05.

**Hypothesis Test Summary**

| | Null Hypothesis | Test | Sig. | Decision |
|---|---|---|---|---|
| 42 | The distribution of CC_Posterior is the same across categories of VAR00001. | Independent-Samples Kruskal-Wallis Test | .131 | Retain the null hypothesis. |
| 43 | The medians of CC_Mid_Posterior are the same across categories of VAR00001. | Independent-Samples Median Test | .315 | Retain the null hypothesis. |
| 44 | The distribution of CC_Mid_Posterior is the same across categories of VAR00001. | Independent-Samples Kruskal-Wallis Test | .427 | Retain the null hypothesis. |
| 45 | The medians of CC_Central are the same across categories of VAR00001. | Independent-Samples Median Test | .537 | Retain the null hypothesis. |
| 46 | The distribution of CC_Central is the same across categories of VAR00001. | Independent-Samples Kruskal-Wallis Test | .785 | Retain the null hypothesis. |
| 47 | The medians of CC_Mid_Anterior are the same across categories of VAR00001. | Independent-Samples Median Test | .915 | Retain the null hypothesis. |
| 48 | The distribution of CC_Mid_Anterior is the same across categories of VAR00001. | Independent-Samples Kruskal-Wallis Test | .742 | Retain the null hypothesis. |
| 49 | The medians of CC_Anterior are the same across categories of VAR00001. | Independent-Samples Median Test | .315 | Retain the null hypothesis. |
| 50 | The distribution of CC_Anterior is the same across categories of VAR00001. | Independent-Samples Kruskal-Wallis Test | .163 | Retain the null hypothesis. |
| 51 | The medians of lhCortexVol are the same across categories of VAR00001. | Independent-Samples Median Test | .185 | Retain the null hypothesis. |
| 52 | The distribution of lhCortexVol is the same across categories of VAR00001. | Independent-Samples Kruskal-Wallis Test | .672 | Retain the null hypothesis. |
| 53 | The medians of rhCortexVol are the same across categories of VAR00001. | Independent-Samples Median Test | .537 | Retain the null hypothesis. |
| 54 | The distribution of rhCortexVol is the same across categories of VAR00001. | Independent-Samples Kruskal-Wallis Test | .718 | Retain the null hypothesis. |

Asymptotic significances are displayed. The significance level is .05.

**Hypothesis Test Summary**

| | Null Hypothesis | Test | Sig. | Decision |
|---|---|---|---|---|
| 55 | The medians of CortexVol are the same across categories of VAR00001. | Independent-Samples Median Test | .537 | Retain the null hypothesis. |
| 56 | The distribution of CortexVol is the same across categories of VAR00001. | Independent-Samples Kruskal-Wallis Test | .703 | Retain the null hypothesis. |
| 57 | The medians of lhCerebralWhiteMatterVol are the same across categories of VAR00001. | Independent-Samples Median Test | .915 | Retain the null hypothesis. |
| 58 | The distribution of lhCerebralWhiteMatterVol is the same across categories of VAR00001. | Independent-Samples Kruskal-Wallis Test | .637 | Retain the null hypothesis. |
| 59 | The medians of rhCerebralWhiteMatterVol are the same across categories of VAR00001. | Independent-Samples Median Test | .915 | Retain the null hypothesis. |
| 60 | The distribution of rhCerebralWhiteMatterVol is the same across categories of VAR00001. | Independent-Samples Kruskal-Wallis Test | .573 | Retain the null hypothesis. |
| 61 | The medians of CerebralWhiteMatterVol are the same across categories of VAR00001. | Independent-Samples Median Test | .701 | Retain the null hypothesis. |
| 62 | The distribution of CerebralWhiteMatterVol is the same across categories of VAR00001. | Independent-Samples Kruskal-Wallis Test | .600 | Retain the null hypothesis. |
| 63 | The medians of SubCortGrayVol are the same across categories of VAR00001. | Independent-Samples Median Test | .915 | Retain the null hypothesis. |
| 64 | The distribution of SubCortGrayVol is the same across categories of VAR00001. | Independent-Samples Kruskal-Wallis Test | .614 | Retain the null hypothesis. |
| 65 | The medians of TotalGrayVol are the same across categories of VAR00001. | Independent-Samples Median Test | .537 | Retain the null hypothesis. |
| 66 | The distribution of TotalGrayVol is the same across categories of VAR00001. | Independent-Samples Kruskal-Wallis Test | .770 | Retain the null hypothesis. |

Asymptotic significances are displayed. The significance level is .05.

**Hypothesis Test Summary**

| | Null Hypothesis | Test | Sig. | Decision |
|---|---|---|---|---|
| 67 | The medians of EstimatedTotalIntraCranialVol are the same across categories of VAR00001. | Independent-Samples Median Test | .537 | Retain the null hypothesis. |
| 68 | The distribution of EstimatedTotalIntraCranialVol is the same across categories of VAR00001. | Independent-Samples Kruskal-Wallis Test | .672 | Retain the null hypothesis. |

Asymptotic significances are displayed. The significance level is .05.

I hereby confirm that this thesis is entirely my own work. I confirm that no part of the document has been copied from either a book or any other source – including the internet – except where such sections are clearly shown as quotations and the sources have been correctly identified within the text or in the list of references. Moreover, I confirm that I have taken notice of the 'Leitlinien guter wissenschaftlicher Praxis' of the University of Oldenburg.

Date, Place: _____ Signature: _____